Undergraduate Responsive Aerial Firefighting Aircraft

A Technical Report submitted to the Department of Mechanical and Aerospace Engineering

Presented to the Faculty of the School of Engineering and Applied Science

University of Virginia • Charlottesville, Virginia

In Partial Fulfillment of the Requirements for the Degree

Bachelor of Science, School of Engineering

Andrew Wheatley

Spring, 2021

Technical Project Team Members

Del Irving

Aaron Huynh

Christopher Kwon

Andy Damm

Jason Le

Leeyung Chang

Matteo Harris

Andrew Wheatley

On my honor as a University Student, I have neither given nor received unauthorized aid on this assignment as defined by the Honor Guidelines for Thesis-Related Assignments.

Jesse Quinlan, Department of Mechanical and Aerospace Engineering

SB-22 Woodzy Owl

Responsive Aerial Firefighting Aircraft

University of Virginia

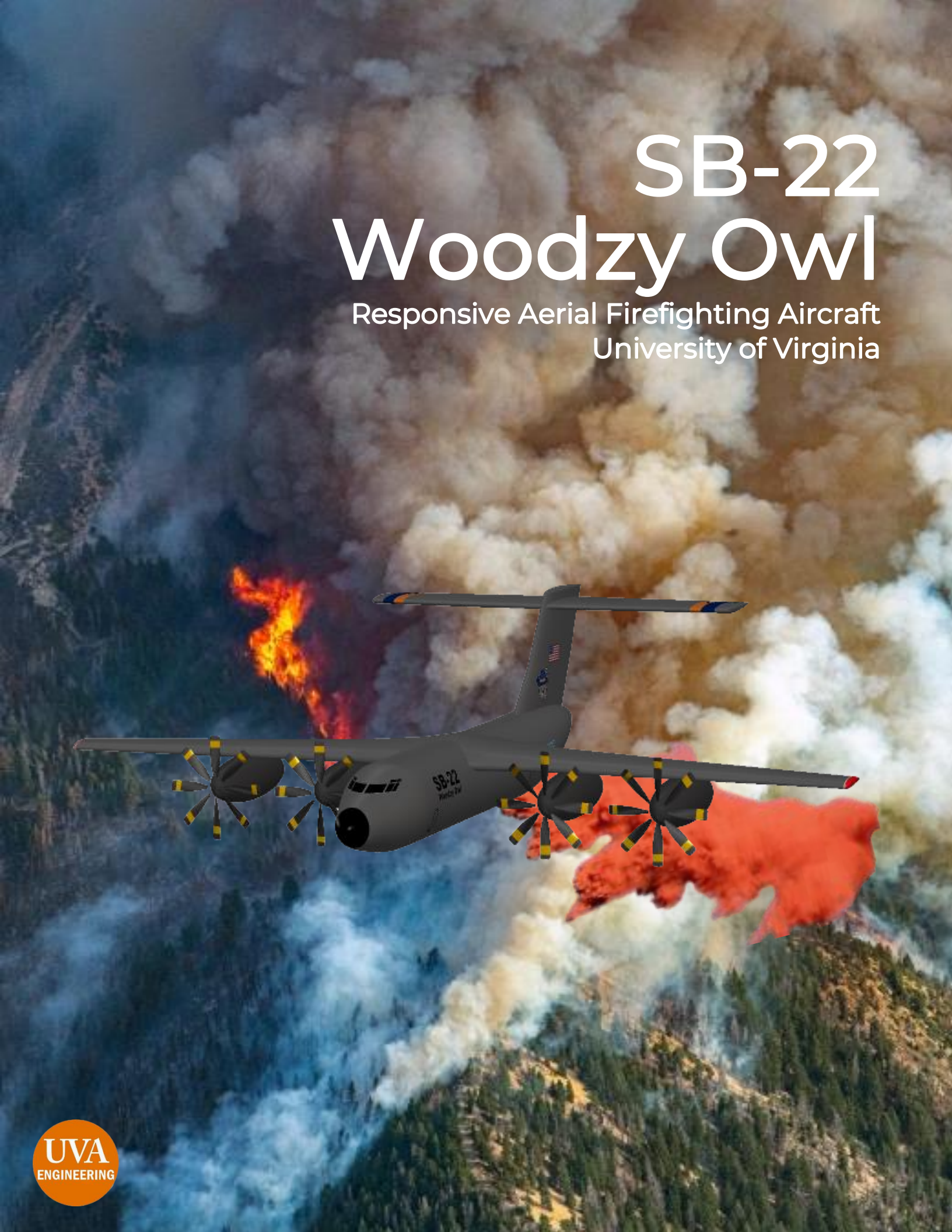

UVA ENGINEERING

AIAA 2021-2022 Undergraduate Responsive Aerial Firefighting Aircraft

Final Design Report

Del Irving, Aaron Huynh, Andrew Wheatley, Andreas Damm,
Christopher Kwon, Jason Le, LeeYung Chang, Matteo Harris

Department of Mechanical and Aerospace Engineering

University of Virginia School of Engineering and Applied Sciences

SB-22 "Woodzy Owl"

MAE 4650/4660 Aircraft Design

Faculty Advisor: Professor Jesse Quinlan

Date of Submission: May 14, 2022

Team Smokey the Bearcraft			
Name	**Email**	**AIAA #**	**Signature**
Delmont Irving	dsi2cd@virginia.edu	1356861	
LeeYung Chang	lwc6tc@virginia.edu	1345959	
Jason Le	jpl4br@virginia.edu	1341618	
Christopher Kwon	cjk8tm@virginia.edu	1255841	
Andrew Wheatley	amw8zp@virginia.edu	1315246	
Matteo Harris	mh2cd@virginia.edu	1357380	
Andreas Damm	akd2yf@virginia.edu	1086449	
Aaron Huynh	ah7pr@virginia.edu	1356835	
Dr. Jesse Quinlan (Advisor)	jrq2a@virginia.edu	306245	

Team Organization & Task Delegation

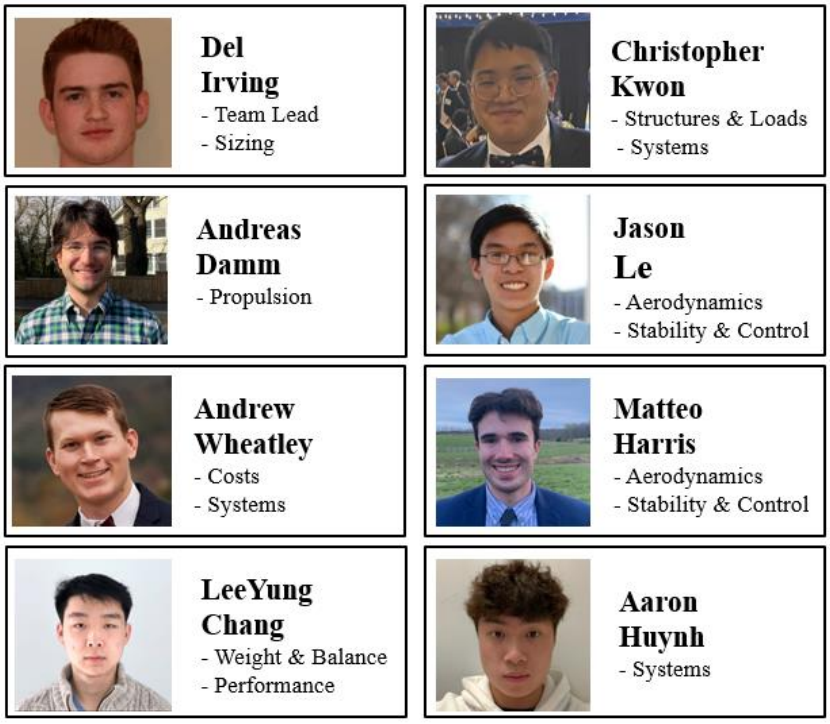

Takeoff Gross Weight	216,000 lb
Operating Empty Weight	126,000 lb
Fuel Burn	11,200 lb
Wing Area	2,525 ft^2
Cruise Lift Coefficient	0.62
Max Cruise Lift Coefficient	1.43
Field Length	7,000 ft
Engine Dry Weight	4,270 lb
Equivalent Specific Fuel Consumption	0.3028 lb/hp/hr
Program Cost	$3.70B

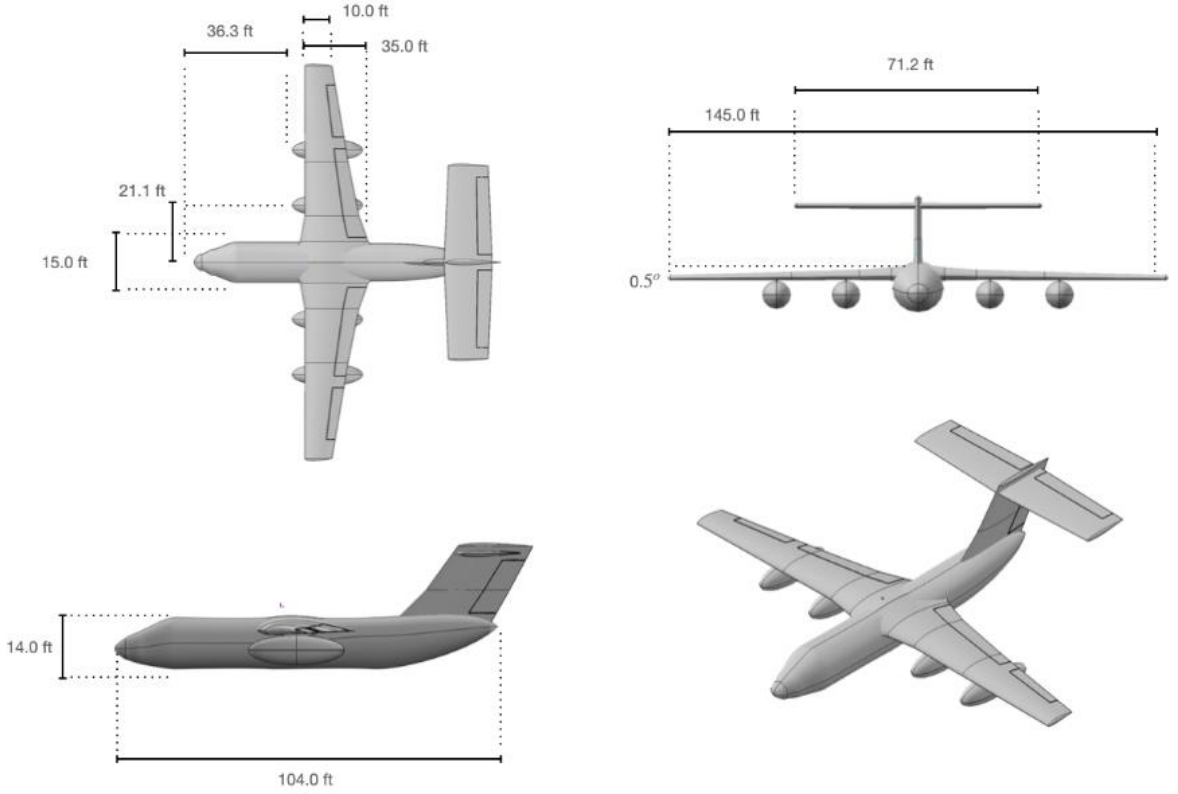

Table of Contents

List of Figures

List of Tables

Acronyms

AAA:	Advanced Aircraft Analysis
AIAA:	American Institute of Aeronautics and Astronautics
AFUE:	Aerial Firefighting Use and Effectiveness
AoA:	Angle of Attack
AR:	Aspect Ratio
CG:	Center of Gravity
EIS:	Entry Into Service
FAA:	Federal Aviation Administration
FEA:	Finite Element Analysis
FLIR:	Forward Looking Infrared
FLOPS:	Flight Optimization System
IFR:	Instrument Flight Rules
KEAS:	Knots Equivalent Airspeed
LAT:	Large Air Tanker
OEW:	Operating Engine Weight
RFP:	Request for Proposal
SFC:	Specific fuel consumption
STOL:	Short Takeoff and Landing
TOGW:	Takeoff Gross Weight
VFR:	Visual Flight Rules
VLAT:	Very Large Air Tanker
YOY:	Year-Over-Year

1. Executive Summary

Wildfire acreage has seen an unprecedented surge in recent years, in large part the result of a smaller number of high-acreage fires (U.S. Forest Service, 2020). As a result, demand for contracted large to very large airtankers (LATs and VLATs) has likewise skyrocketed (U.S. Forest Service, 2020). Current airframes used in aerial firefighting are largely repurposed passenger aircraft and transports. This results in significant airframe variation, a need for retrofitting and consequent compromises and inefficiencies, and high loads and fatigue on already high-flight-hour airframes.

The AIAA request for proposal (RFP) for this year's design challenges aims to address the need for an airframe to meet these more stringent requirements by detailing requirements for a purpose-built LAT with a minimum of 4,000 gallon capacity capable of multiple drops, a mission radius of at least 200 nautical miles, a 2,000 nautical mile ferry range, 300 knot dash speed after payload drop, takeoff within 8,000 feet balanced field length, and an entry into service (EIS) by 2030 (AIAA, 2021). In addition, the RFP sets out the need to maintain VFR and IFR flight, icing stability, FAA 14 CFR Pt. 25 compliance, and qualitative objectives of minimizing costs, maximizing reliability, and maximizing ease of maintenance (AIAA, 2021).

This report details the development of the SB-22 "Woodzy Owl" to address the request for a new, purpose-built LAT, compliant with firefighting aircraft demands outlined in the RFP (AIAA, 2021).

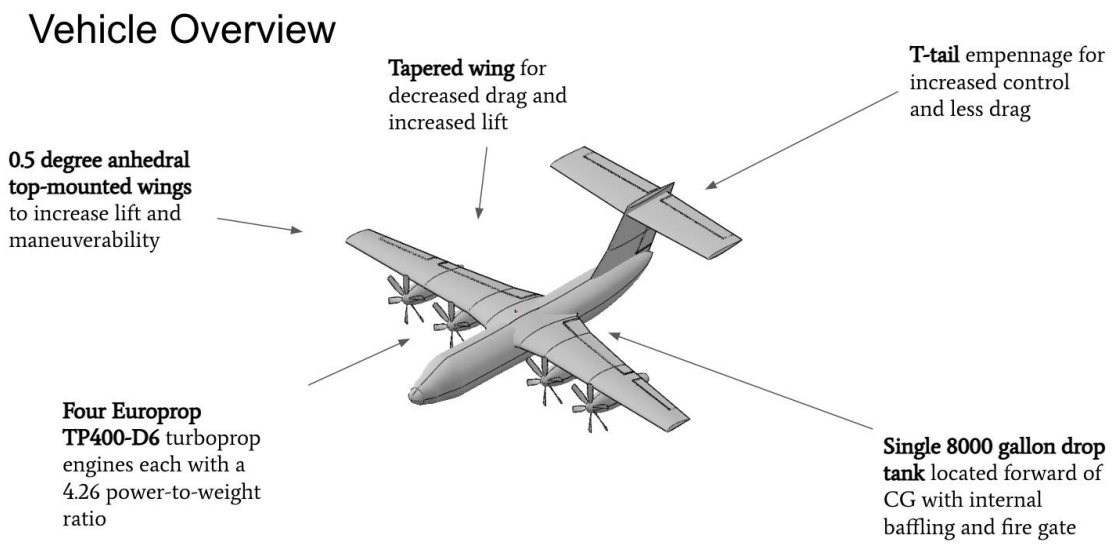

Figure 1. Design Overview of the SB-22 "Woodzy Owl", highlighting details and capabilities.

The SB-22, designed to meet or exceed RFP requirements, is discussed in detail in this paper. The proposed aircraft has an 8,000 gallon capacity, a 200 nautical mile mission radius at maximum load, and uses technology current enough for a projected 2030 EIS. It is expected to have a takeoff gross weight of approximately 216,000 lb. and empty weight of approximately 126,000 lb. Program cost is projected to be approximately $3.7 billion and to feature an exceptionally variable fly-away cost, with estimates from $258 million to $25.8 million dependent on production scaling, and an estimated cost per flight hour of $8,267.

2. Introduction

Annual data collected by the U.S. government has shown recent (5-10 year) general trends, in which annual wildfire numbers have been in slight decline, but annual acreage burnt has been on a steady increase (National Interagency Coordination Center, 2020). While "exclusive use" air tanker contracting has remained steady, year-over-year use of contracted large and very large air tankers has seen an increase in line with increased fire prevalence, with these "surge" aircraft used to address demand as necessary (National Interagency Coordination Center, 2020)

Table 21 – CY 2016-2020 CWN LAT Use Summary

Calendar Year	Flight Hours	Retardant (gallons)
2016	414	1,662,021
2017	395	1,658,126
2018	1,196	4,194,568
2019	608	2,047,461
2020	3,707	11,706,065
5-yr average	**1,264**	**4,253,648**

Table 22 – CY 2016-2020 CWN VLAT Use Summary

Calendar Year	Flight Hours	Retardant (gallons)
2016	52	595,995
2017	199	1,991,424
2018	291	1,970,183
2019	55	316,319
2020	570	4,042,116
5-yr average	**233**	**1,783,207**

.

Figure 2. Tables from the U.S. Forest Service 2020 Aviation Annual report indicating year-over-year (YOY) use of contract-when-needed (CWN) aircraft in the LAT (large air tanker) and VLAT (very large air tanker) categories, 2016-2020

At present, 7 LAT and 2 VLAT types are described in the Annual Fuel Utilization Efficiency (AFUE) report (United States Department of Agriculture, 2020). With respect to the AIAA RFP the aircraft which operate in the larger-than 4,000 gallon range are the purpose-

modified EC-130Q and 737-300 LATs, and the DC-10 and 747-400 VLATs (United States Department of Agriculture, 2020). Broadly speaking, the aircraft in the LAT/VLAT category are old military and civil transport aircraft with modifications made by independent contractors, who are in turn contracted by the U.S. Forest Service to operate in the air attack role (United States Department of Agriculture, 2020). Also in this category are aircraft such as military C-130s equipped with Modular Airborne Fire Fighting Systems (MAFFS), and scooper type aircraft including the Canadair CL-415, which represent modular firefighting-adaptable aircraft and water-scooping aircraft respectively – the former is crewed by service members and the latter is a purpose-built aircraft flown by contractors (United States Department of Agriculture, 2020).

In operational studies, compromises from using adapted airframes over clean-sheet designs are observed. The most critical is the specter of extreme loading conditions, a matter of significant concern for some time. A 1988 study featuring some 2763 drops from the previous 5 years, focused on the C-119 aircraft, found 90% of drops to exceed maximum drop airspeeds, and a further 25% to exceed 2.5g peak acceleration (George, 1988).

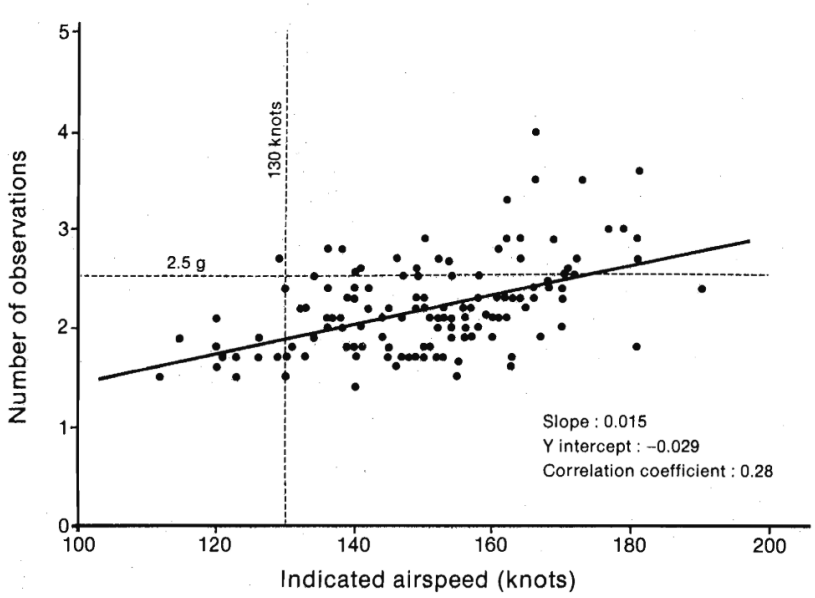

Figure 4. Distribution of drops in relation to the 130-knot maximum airspeed and 2.5-g peak acceleration criteria.

Figure 3. Figure 4 from ORE Update (George, 1988)

A more recent study, a Blue Ribbon Panel report for the Forest Service, found stress problems like those previously observed, citing key concerns including lack of maintenance parts, longer wildfire seasons, and larger-scale fires, all of which impact airframe life (Hall et al., 2002). Alarming even as anecdotes, the study notes incidents wherein aircraft reached load factors of up to 3.9 g, wing cracks reached some 13 inches, and a single crack exhibited 5 inches of growth over the span of a single day (Hall et al., 2002). The extreme conditions which result in the airframe fatigue described underscore the critical need for a purpose-built firefighting aircraft adapted to the demands of the aerial firefighting mission.

3. Requirements, Goals, and Missions

In this section, the main requirements and mission parameters influencing the final design of the SB-22 "Woodzy Owl" are discussed. This section includes the mandatory requirements and objectives outlined by the AIAA RFP as well as requirements derived from the nature of the design firefighting mission, which necessitates a VLAT dropping thousands of gallons of retardant at low speeds and low altitudes. The mission design for both the firefighting mission and a ferry mission are then outlined. Finally, the environmental concerns of the mission are discussed, particularly temperature and altitude fluctuations specific to the fire response mission setting, and specific system design requirements to address these concerns are enumerated.

3.1. RFP Requirements

In this section, the driving requirements and objectives selected for this aircraft design project are listed as outlined by the RFP provided by the American Institute of Aeronautics and Astronautics. These can be found in Tables 1, 2, and 3 which list General Requirements, Design Mission Requirements (for both firefighting and ferry missions), and the Certification Requirements, respectively, within the RFP.

Table 1. General Requirements for a Firefighting Aircraft from the AIAA

Requirement	Comments
EIS by 2030	Mandatory Requirement
Use of existing engine(s) or engine(s) with entry into service 2 years prior to aircraft EIS	Mandatory Requirement
Documented assumptions of specific fuel consumption/efficiency, thrust/power, and weight	Mandatory Requirement
Fire Retardant Capacity of 8,000 gallons	Objective or Goal
Multi-drop capable (min 2,000 gallons per drop)	Mandatory Requirement
Fire Retardant Reload ≥ 500 gal/min	Mandatory Requirement
Retardant Density ≥ 9 lbs/gal	Mandatory Requirement

Table 2. Design Mission Requirements for a Firefighting Aircraft from the AIAA

Requirement	Comments
Payload Drop Speed ≤ 150 kts	Mandatory Requirement
Payload Drop Altitude ≤ 300 ft AGL	Mandatory Requirement
Design Radius (Full Payload) of 400 nmi	Objective or Goal
Design Ferry Range (No Payload) of 2,000 nmi	Mandatory Requirement
Dash Speed (After Payload Drop) of 300 kts	Mandatory Requirement
Balanced Field Length ≤ 8,000 ft @ 5,000 ft MSL elevation on a +35°F hot day	Mandatory Requirement

Table 3. Certification Requirements for a Firefighting Aircraft from the AIAA

Requirement	Comments
Capable of VFR and IFR flight with an autopilot	Mandatory Requirement
Capable of flight in known icing conditions	Mandatory Requirement
Meets applicable certification rules in FAA 14 CFR Part 25	Mandatory Requirement

3.2. Design Goals

The RFP outlines several design objectives to be met or otherwise optimized for in the final aircraft design. First, operations and support costs are to be minimized - one specifically mentioned method is by designing modularity into the structure and key components, so that ease of repair and availability of replacement parts are maximized in the context of a chosen

support strategy. The production cost is also to be minimized by choosing materials and manufacturing methods appropriate for the annual production rate based on analysis of the potential market size. Additionally, since all current firefighting aircraft are commercial or military aircraft retrofitted with firefighting equipment, the design of an aircraft for the full purpose of firefighting should have a level of reliability and operational availability equal to or better than comparable firefighting aircraft (Langfield, 2021, para. 1). Along the same lines the aircraft maintenance should be equal to or better than comparable aircraft, including failure rate and time to repair. The RFP also notes a few other features that should be considered, such as ensuring that flying qualities meet CFR Part 25, identifying system functionality and components necessary for the aircraft to fly in both controlled and uncontrolled airspace, listing all required equipment, and considering necessary features compared to those that are up to the wishes of the customer (AIAA, 2021, p. 1-3).

Apart from the design objectives laid out in the RFP, the team has laid out several derived requirements that are based on goals for the design that are not explicitly stated but are necessary for the aircraft based on the nature of the mission. The main consideration is designing an aircraft that will be suited for ‘low and slow’ flight during the period where the fire retardant will be released. Although there are metrics laid out in the Design Mission Requirements in Table 2 for the maximum payload drop speed and maximum drop altitude, a low and slow drop will also be necessary for precise and effective aerial firefighting in order to contain the flames and assist the smaller droppers and human firefighters on the ground.

With such a large aircraft approaching ground level at a low speed, it will be necessary for the design to feature lift capabilities that allow the VLAT to regain altitude after payload release. Additional considerations include that a release of 2,000 gallons of fire retardant at a

time could significantly impact the CG of the aircraft as well as creating a design where the release of mass amounts of retardant is not ingested by the engines which has been known to cause lasting damage (Gabbert, 2014, para. 1).

3.3. Mission Design

A design was constructed for a firefighting mission including multi-drop capability per the RFP, as well as for a ferry mission carrying no payload that must meet the mandatory required ferry range of 2,000 nautical miles. First for the firefighting mission the aircraft will satisfy a balanced field length of 8,000 feet as specified in the RFP. The balanced field length describes the length of runway available so that if the aircraft accelerated to V_1 and experienced engine failure, the takeoff could be rejected, and the aircraft would stop on the runway at maximum gross weight. This balanced field length also describes the length of runway necessary if the engine failed and takeoff was not rejected. If V_1 is lower, meaning engine failure occurs sooner at a lower speed, it will take longer for the aircraft to reach the rotation point (takeoff) with less thrust. On the other hand, if V_1 is high, meaning the aircraft were traveling fast when engine failure occurred, the plane has already achieved enough speed to takeoff and thus the balanced field length is about the same. This is the opposite for a rejected takeoff where higher V_1 means a longer time to stop and a lower V_1 means a shorter time to stop (PilotClimb, 2021, para. 1-16).

After successful takeoff, the aircraft will climb to the cruise altitude of 10,000 ft and cruise for 200 nmi once this altitude is reached. After this cruise segment the aircraft will descend in preparation for the first payload drop of fire retardant onto the target. The drop will then occur at the RFP specified 300 ft above ground level. Following the initial drop the aircraft will then loiter in preparation for a second payload drop, which will again occur at 300 ft above

ground level. This section of the mission design may be modified for various firefighting applications.

Although the RFP specifies the possibility for multiple payload drops, scenarios where the full 8,000 gallon fire retardant capacity is necessary in one drop may arise. In FLOPS the mission design simulated a more complex profile featuring four separate drops with 2,000 gallons of fire retardant released at each to consume the entire fire-retardant capacity during the mission. The drop portion of the mission design is highly dependent on the nature of the fire, but the drop system has the fire-retardant capacity and the multi-drop capable system adept for handling any situation. Following the drop portion, the aircraft will again climb to cruising altitude of 10,000 ft, completing the same 200 nmi dash back upon reaching cruise altitude. Once this cruise segment has been completed, the aircraft will descend and loiter until landing. The mission profile and expected speeds and distances for the mission stages are summarized in Table 4.

Table 4. Firefighting Mission Profile

Mission Stage	Speed (ft/s)	Distance	Notes
1: Takeoff	278.3	8000	Balanced field length (ft)
2: Climb to Cruise	-	-	10,000 ft alt
3: Cruise	506	200	nmi
4. Descend	-	-	-
5: Drop 1	253	-	300 ft AGL
6: Loiter	-	-	-
7: Drop 2	253	-	300 ft AGL
8: Climb to cruise alt	-	-	-
9: Dash back	506	200	nmi
10: Descend	-	-	-
11: Loiter	-	-	-
12: Land	328.9	8000	Balanced field length (ft)

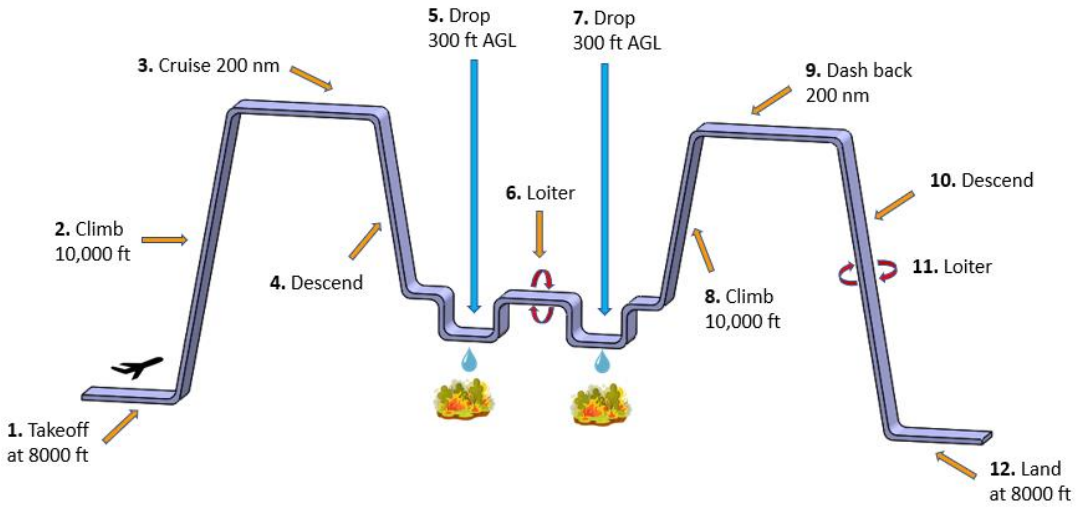

Figure 4. Firefighting Mission Profile for the SB-22 "Woodzy Owl"

For the ferry mission, the aircraft will operate without the 8,000 gallon fire retardant capacity, greatly reducing takeoff gross weight yet still taking off from the same 8,000 ft balanced field length. In the event of engine failure at V_1 the aircraft will safely be able to stop before the end of the runway with significant stopping distance due to this initial reduction in TOGW. Upon a successful takeoff, the aircraft will then climb to a cruising altitude of 30,000 ft, compared to the 10,000 ft cruise altitude for the firefighting mission design. Once this altitude is achieved, the aircraft will cruise for 2,000 nmi per the RFP design ferry range. At the end of this cruise segment the aircraft will begin a descent and then loiter shortly before landing again on the 8,000 ft balanced field length. The ferry mission profile and expected speeds and distances are summarized in Table 5.

Table 5. Ferry Mission Profile

Mission Stage	Speed	Distance	Notes
1: Takeoff	278.3 ft/s	8000 ft	Balanced field
2: Climb to Cruise	-	-	30,000 ft alt
3: Ferry Cruise	430.1 ft/s	2000 nmi	
4: Descend	-	-	-
5: Loiter	-	-	-
6: Approach & Land	328.9 ft/s	8000 ft	Balanced field

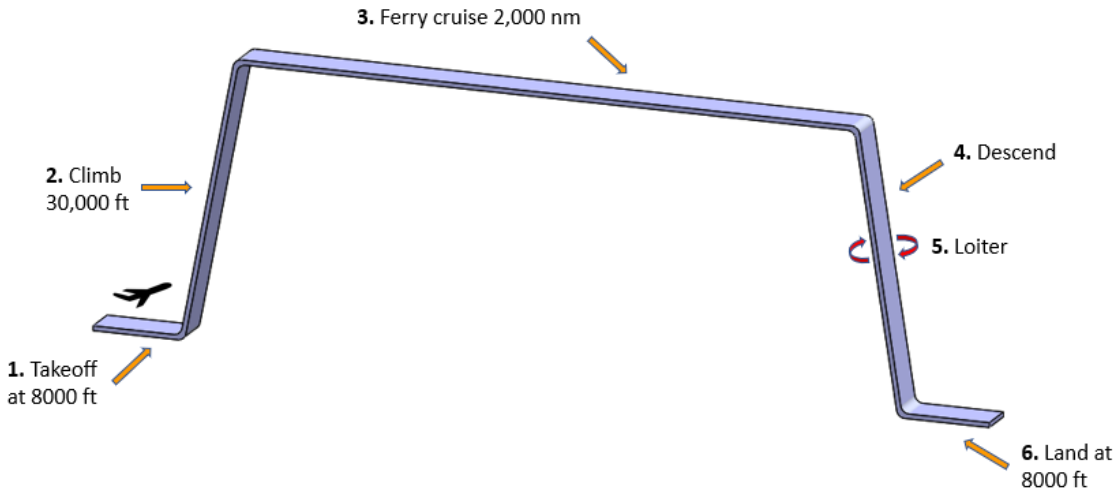

Figure 5. Ferry Mission Profile for the SB-22 "Woodzy Owl"

3.4. Mission Environment

This section of the report focuses on the potential environmental concerns present during an aerial firefighting mission. In general, VLATs are part of a greater fleet of aerial firefighting response vehicles and stand as a last resort option due to the high fly away cost compared to smaller aircraft in the fleet or vertical lift vehicles. For this reason, it is generally assumed that VLAT will only respond to large forest fires that spread across vast distances or threaten more urban areas. The Woodzy Owl will thus have to be able to take off and land on a variety of runway conditions, from structured airports to rural dirt runways. Shifting to considerations during flight, it is known that lifting capability is dependent on temperature and elevation, both of which will drastically vary during an aerial firefighting mission.

Temperatures at the cruising altitudes for both the firefighting profile and ferry profile as seen in Figures 4 and 5 are at an elevation that may induce known icing conditions, and yet upon dropping payload at only 300 ft above ground level the flames from the fire may roar high enough to significantly increase temperatures on the aircraft. According to the Natural History Museum of Utah, extreme forest fires may burn up to 165 feet or more and reach temperatures exceeding 2,192°F (p. 2). At the required drop altitude, the aircraft is not directly in the inferno, but temperatures that high at less than 150 feet from the aircraft are significant enough that this factor should be considered during the design process.

The last consideration that arises from the mission environment is the fact that although flames may not reach the drop altitude of the aircraft, treetops might extend into this drop zone (California Department of Parks and Recreation, 2022, para. 1). This means the drop zone may occur in the midst of the treetops, and as a result the plane structure should be designed in order to avoid any significant damage as a result of any collision while attempting to release the payload. The height of these trees also adds the consideration that although flames on the ground cannot reach up to the drop height, a tree which is ablaze can allow the fire to reach altitudes closer to the aircraft, increasing the average temperature at this height. All of these environmental factors should be considered during the design process, influencing a system that has high lift capabilities, high mounted features such as the wings and empennage to avoid collision with treetops, and auxiliary systems capable of handling the temperature variation innately present in the mission design.

4. Design Approach

In the initial design process, each member of the team generated a rough conceptual outline of an aircraft design, from which three concepts were selected for further development. Designs were generated in OpenVSP by each group member, brought to a group meeting, assessed, and down-selected to the three most viable candidates. The initial concepts were as follows:

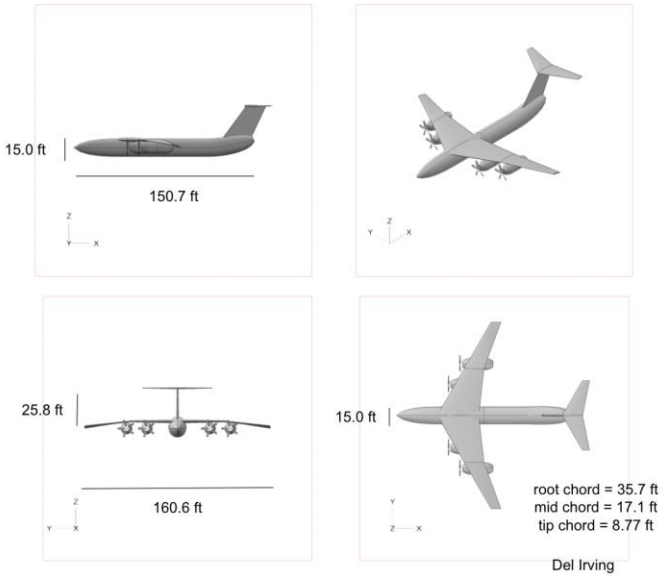

Figure 6. Conceptual Design #1 from Del Irving

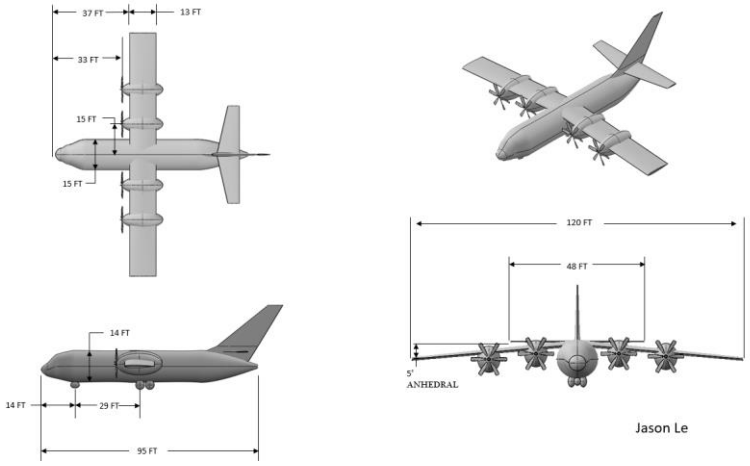

Figure 7. Conceptual Design #2 from Jason Le

Of the initial concepts above, a common theme presents itself, that of a multi-engined transport with limited wing sweep. In particular, many models are derived from turboprop military transports, such as the C-130.

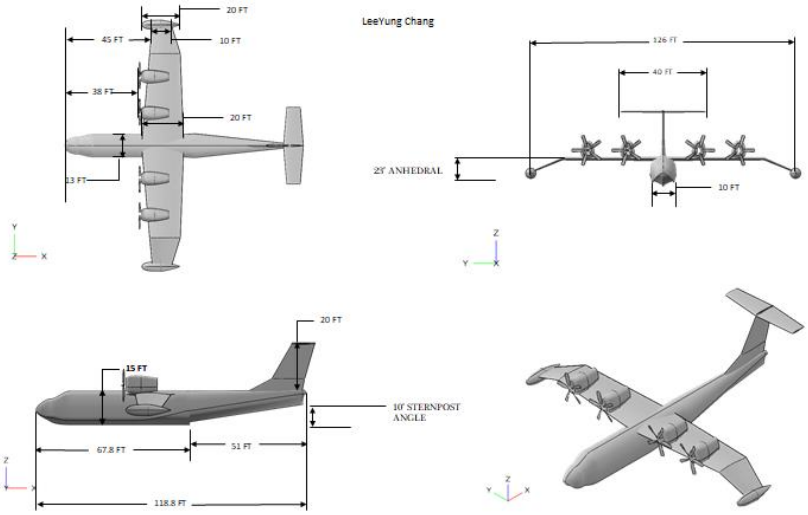

Figure 8. Conceptual Design #3 from LeeYung Chang

Aaron Huynh:

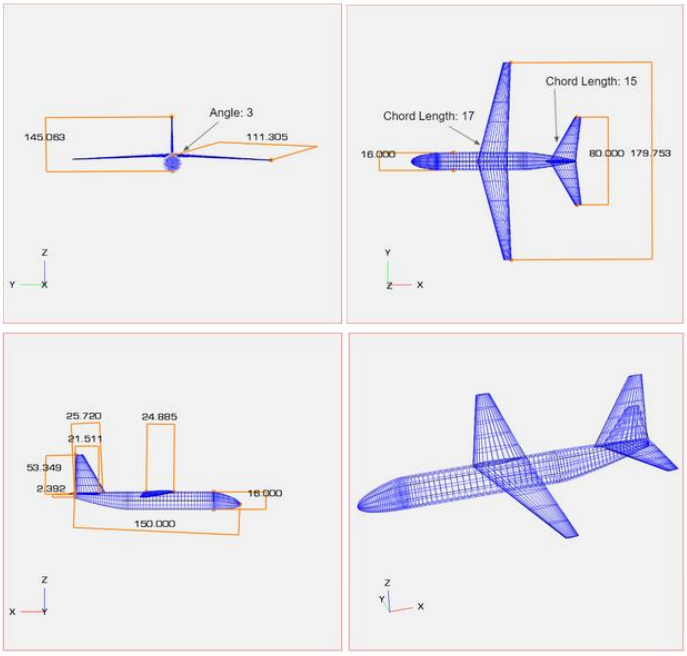

Figure 9. Conceptual Design #4 from Aaron Huynh

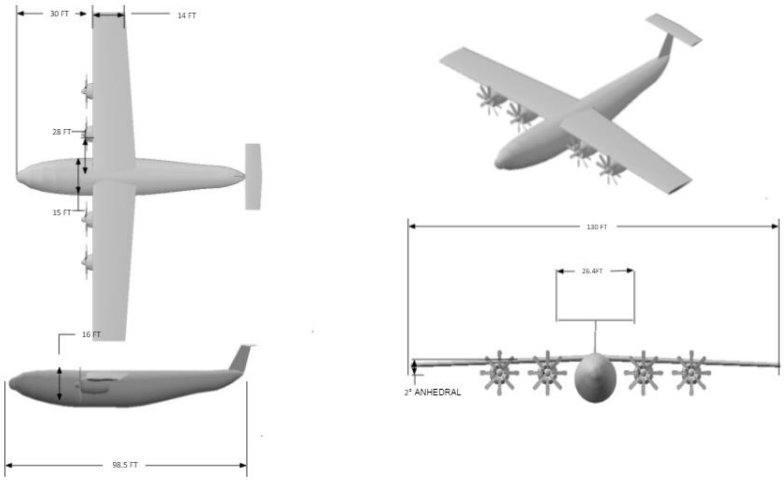

Figure 10. Conceptual Design #5 from Andrew Wheatley

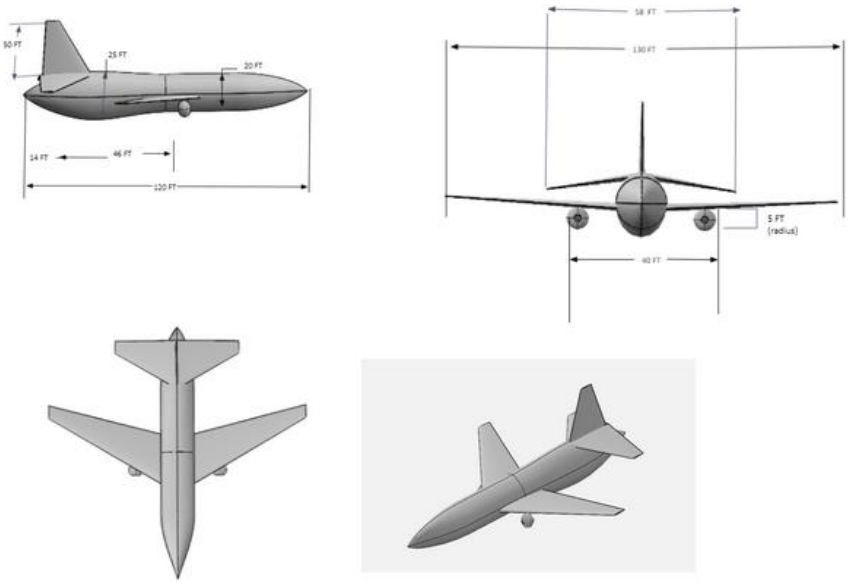

Figure 11. Conceptual Design #6 From Matteo Harris

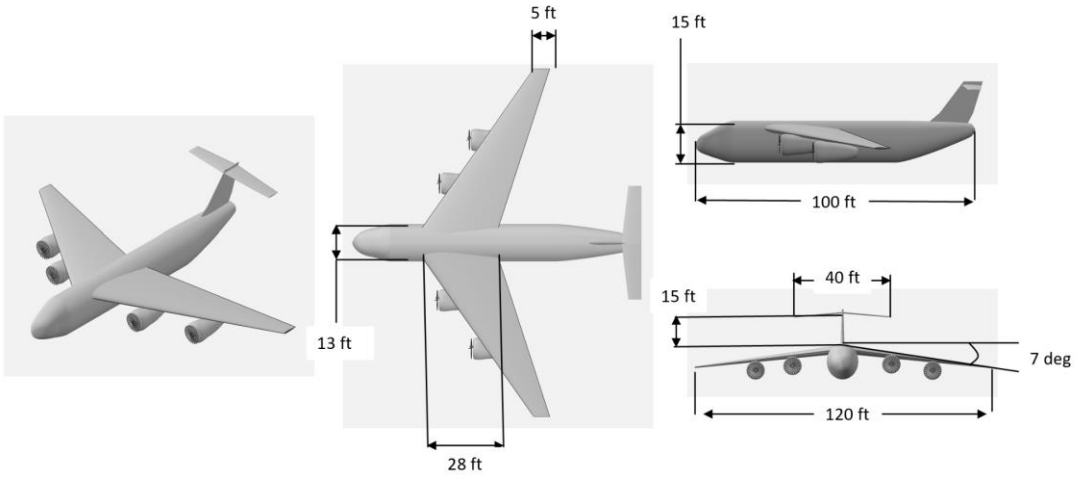

Figure 12. Conceptual Design #7 From Christopher Kwon

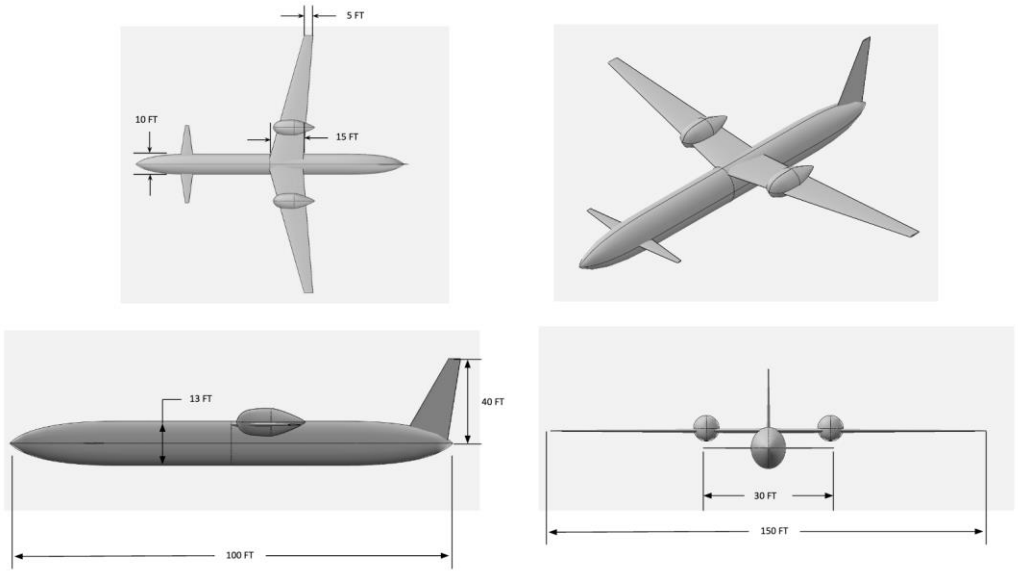

Figure 13. Conceptual Design #8 From Andreas Damm

In down-selecting, a focus was placed on enabling ‘low and slow’ operation, i.e. the conditions under which the water bombing stage of the aerial firefighting mission occurs. To this end, a high wing was prioritized, with the chief concern being stability, and a secondary thought being that the slight reduction in ground effect would have an effect of decreasing landing distance to a limited degree. Other attributes leading to selection of a high wing were minimizing

ingestion of fire retardant by engines, minimizing any potential detrimental effects on control surfaces due to retardant, and increasing the field of view for pilots during the drop stage as much as possible. To a certain extent this likewise affected engine placement, with one of the selected designs using a top-mounted engine primarily to avoid liquid intake. Another aspect of the wing prioritized was a higher planform area, in order to continue to reduce stall speed and increase capability for that 'low and slow' type mission. At this initial stage, a wide range of wing shapes existed so far as taper, sweep, and twist; future down-select stages allowed incorporations of unique attributes of each design into a final product.

Another matter of interest was the control surfaces, specifically the empennage shape. The designs above featured vertical and horizontal stabilizers; the major difference was in horizontal as opposed to vertical stabilizers, with a brief digression into canards - the latter was discussed briefly before a consensus that the added complexity and lack of precedence made it an unsuitable option for this particular project. Both T-tail and conventional tails were incorporated into the down-select as at this stage it was considered desirable to take both options for future trade studies.

With respect to sizing, the primary sizing factor was thought to be payload - as at this stage payload was yet to be determined, and sizing was likewise uncertain, a very qualitative check based on approximate size matching to current firefighting aircraft was undertaken, with the expectation that sizing exercises would be carried out in detail in the future.

The first design selected was a turboprop with high mounted anhedral swept wings and a large T-tail, inspired by the Ilyushin Il-76, a Russian aircraft used for aerial firefighting. The high lift generation, visibility of the open cockpit, and large T-tail were seen as advantages for maximizing control and stability, while the swept wing was a design element with some merit as

a comparative element to the other swept-wing selections. The T tail is commonly seen in transport aircraft, such as the Lockheed C-130 and Boeing C17, where access to the payload is at the rear of the fuselage.

The second initial design selected was based on the C-130, and likewise featured a high anhedral wing with four turboprops, but had a straight wing, providing one avenue of direct comparison with the former design. The most significant fundamental difference other than wing sweep was the low-mounted cruciform tail, which presented a difference from the T-tail of the first design. A cruciform tail configuration was selected as a compromise between a conventional and T-tail. The horizontal tail is slightly above the wing flow wake for enhanced horizontal stabilizer efficiency. This location also helps avoid the additional loads on the vertical tail when the horizontal tail is at the top. This design similarly had advantages in generating lift and control, as well as some degree of (relatively) short landing and takeoff distance.

The third initial design selected was loosely based on the Shinmaywa US-2, a Japanese amphibious aircraft. This design featured a “scooper” capacity akin to that of the Canadair CL-415, with the ability to skim the surface of the water and rapidly refill by “scooping” from the surface into an internal reservoir. The major complication present in this design was the RFP need for retardant to be mixed into the tank, which would have presented an obstacle - an internal reservoir of retardant concentrate and use of a pump with mixing capacity would have been one method of mitigating this trade-off. The seaplane characteristics of this aircraft resulted in the use of a high-mounted wing and T-tail, here presenting an additional advantage of establishing greater distance away from the spray generated in seaplane takeoff and landing. To this end the aircraft features top-mounted turboprop engines, which provide some separation from spray released both in seaplane flight and in dropping fire retardant. The wingtips are

canted downward and end in floats, which necessitate increased wing durability to handle the associated stresses applied during landing and taxiing.

In early operations research, it was concluded that the added weight and water dependence of the seaplane made it ill-suited for the RFP. While the refill rate and other operational details of the aircraft were impressive, the major increase in weight of the reinforced airframe needed for seaplanes, in addition to the onerous maintenance costs and hours associated with waterborne craft and corrosion considerations, posed significant disadvantages in areas the RFP considered. In addition, the dependence on a large body of water for refill, and potentially basing if the aircraft was to be amphibious instead of strictly a seaplane, presented a degree of uncertainty as to whether the aircraft as designed would be able to reach and take care of a fire - if said fire was too far from a body of water, the distinct possibility of the craft being useless made it a poor design choice. As a result, the choice was narrowed down to the first two initial designs, with elements of each being incorporated into the finalized ‘baseline’ design from which elemental trade studies were done.

This baseline craft tentatively featured the high T-tail of the first design, but the mostly unswept wings and general fuselage shape of the second design, the C-130 derivative.

5. Sizing Analysis

5.1. Initial TOGW Estimation

The initial takeoff gross weight served as the starting point for the design of the aircraft. The weight estimate is driven by the RFP mission requirements and historical weight data for similar classes of aircraft. To determine the initial TOGW, the fuel weight fraction method was used from *Fundamentals of Aircraft and Airship Design: Volume 1* by Nicolai and Carichner. These fuel weight ratios were estimated for each flight phase as defined in the firefighting mission profile. The estimation method employs equations 1 and 2 for available empty weight and required empty weight, respectively:

$$W_{empty\ avail} = W_{TO} - W_{fuel} - W_{fixed} \quad (1)$$

$$W_{empty\ required} = 0.911 * {W_{TO}}^{0.947} \quad (2)$$

Equation 2 is based off of historical trends for bomber and transport aircraft types. W_{fixed} was estimated to be 36,280 lb and the initial W_{TO} was estimated at 236,237 lb. W_{fuel} is calculated from the product of the fuel fractions from each flight phase. A summary of the initial fuel weight fractions is shown in Table 6 below.

Table 6. Initial Fuel Weight Fractions

Mission Stage	Fuel Weight Ratio	Value
Takeoff	W2/W1	0.97
Climb to Cruise	W3/W2	1
Cruise	W4/W3	0.992
First Drop	W5/W4	0.99
Dash to Loiter	W6/W5	0.975
Loiter	W7/W6	0.961
Second Drop	W8/W7	0.99
Dash to Cruise	W9/W8	0.975
Cruise	W10/W9	0.931
Landing	W11/W10	0.97

W_{fuel} is calculated with Equation 3:

$$W_{fuel} = (1 + reserved + trapped) * (1 - W11/W1) * W_{TO} \quad (3)$$

The reserved and trapped fuel is assumed to be 0.05 and 0.01 (Nicolai & Carichner, 2010). W11/W1 is the product of all of the fuel weight ratios from the table above. Now $W_{empty\ avail}$ and $W_{empty\ required}$ can be calculated and plotted by iterating on the W_{TO} estimate. These computations were repeated until $W_{empty\ avail}$ and $W_{empty\ required}$ converged and resulted in a TOGW estimate of 136,872 lb , as seen in Figure 14. This weight fuel fraction method is a very rough initial estimation procedure that served as a guide for early decision making in the design process. More detailed weight estimates were performed in FLOPS during the later stages of the design, where the final TOGW was determined.

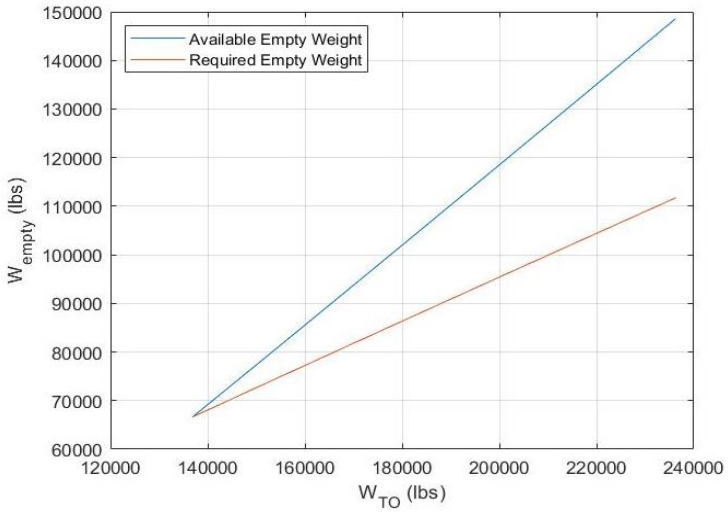

Figure 14. Empty Weight vs. TOGW

5.2. Constraint Diagram

The initial sizing of the aircraft was determined based on performance constraints set by the AIAA RFP. A constraint diagram was constructed based on rate of climb, dash speed, takeoff, and landing constraints derived from the RFP, as seen in Figure 15.

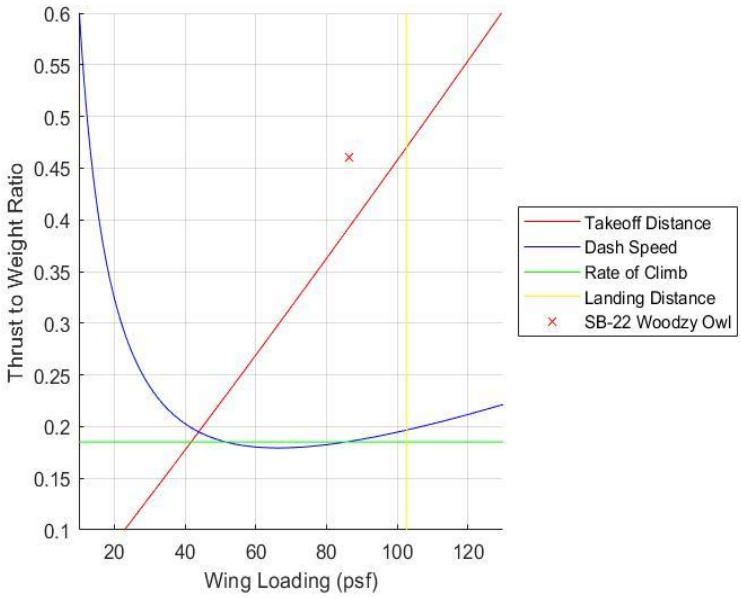

Figure 15. Constraint Diagram

The design space consists of the region to the left of the landing distance line and above the takeoff distance and dash speed curves. Initially, the team wanted to minimize the wing loading and the thrust-to-weight ratio as much as possible at the point of intersection between the takeoff distance and dash speed curves. However, upon further research of comparator aircraft like the C-130 and as the team went deeper into the design of the aircraft, it was realized that the wing loading needed to be higher to satisfy mission requirements. The team decided to then anchor the wing loading at 90 psf and iterate on the design from there. This value came from the wing loading trend range of 40-90 psf for STOL and utility transports from Nicolai's textbook, with similar aircraft being closer to the upper range. The final design resulted in the location of the red 'x' in the constraint diagram, with a wing loading of 85.70 psf and a thrust to weight ratio of 0.46.

6. Propulsion

The approach adopted by the team in selecting an engine to suit the prospective design involved making initial decisions based on mission constraints and analysis of comparator aircraft, and then using software tools to develop more rigorous metrics for comparing prospective engine decks. In section 6.1, the initial stages will be outlined, documenting the rationale behind decisions made in engine selection. Then, section 6.2 will provide a more detailed rundown of the performance characteristics of the engine, and various trade studies conducted to further hone the engine design for the air tanker application.

6.1. Engine Selection

In section 3, a final top-level mission profile was derived for a large-very large air tanker capable of a multi-retardant-drop mission. Using this mission specification, a top-level analysis of the benefits of various aircraft engines was conducted to narrow down the kind of engine that would best suit the firefighting application. Certain engine configurations were quick to be dismissed; for example, an easy decision was to only consider air breathing engines, as any rocket-based propulsion would certainly be overkill for the low-speed scenario. Moreover, within air breathing models, configurations like ramjet and scramjet are equally ill-suited for low-speed, heavy aircraft. Finally, between a turbofan and a turboprop configuration, the final decision was made to opt for the turboprop engine, because of its high efficiency in the low- to mid-subsonic flight regime (Nicolai, 2010, p. 436). Since low speeds are required to execute the precise dropping maneuver, and the cruise will be conducted at relatively low speeds, this heightened efficiency would have a large impact throughout the flight envelope. Turboprop engines are also capable of producing large amounts of lift at takeoff by subjecting the wing to

its slipstream, which is beneficial in meeting the restrictions placed by the RFP on balanced field length.

It is also worth briefly mentioning that an electric or hybrid propulsion system was considered by researchers. However, due to limitations in battery technology and the large amounts of space and weight taken up by the additional batteries and motors, such a design was deemed unfeasible for the size of the SB-22 and the timeline of design entry into service by 2030. With that being said, the integration of electric systems into aircraft design is critical for achieving carbon neutrality in the aviation industry. Nevertheless, with the current state of the technology, there is no realistic way of achieving an electric propulsion design in any capacity for the large to very large air tanker class plane.

After closing in on the turboprop configuration, current models in use by similar large and low speed aircraft were compiled, and various performance metrics were tabulated for comparison. Table 7 below documents the data collected for each potential pre-existing engine which could be fitted into our aircraft configuration.

Table 7. Preliminary Turboprop Data

Engine	Dry weight (lb)	Max power output (hp)	Power-to-weight ratio	Specific fuel consumption (lb/hp*h)
NK-12MV	6393	15000	2.346	0.36
TP400-D6	4189	11000	2.626	0.3748
Tyne 21	2392	6100	2.55	0.4899
Allison T56	1940	5250	2.706	0.469
AE2100	1742	4637	2.662	0.4603

Primary metrics of importance highlighted by researchers in the further down-selection for the engine were power-to-weight ratio and SFC. In addition to seeking an engine with a high value in each of these metrics, the team also required an engine with enough raw power to support the large airframe and heavy load carried by the aircraft. The NK-12MV, though boasting a high raw power, also came at an exceptionally large weight and the weakest fuel

consumption compared to the other engines. The added cost of the additional weight and fuel requirements, as well as that level of power being deemed exorbitant even for the tanker application, meant the NK-12MV was quickly eliminated. Between the other four aircraft, the Tyne 21, Allison T56, and AE2100 all feature very high SFC, max power of around 5,000-6,000 hp, and dry weight of 1,500-2,500 lbs. Between these three, since they were all relatively close in these performance parameters, the Allison T56 was chosen as the best of the three for having the highest power-to-weight ratio.

Through this elimination process, the two engines which remained were the TP400-D6 and the Allison T56. The latter has significantly better SFC and a slightly better power-to-weight ratio, but the concern is that in terms of raw power, the engine will not be enough for this size of the proposed aircraft. In order to come to a final decision on the engine, a preliminary GasTurb model was developed for a takeoff configuration for each of the engines. This preliminary data would be compiled and transferred into the mission profile derived in FLOPS, and overall mission parameters of takeoff gross weight and block fuel burn can be compared. For the TP400-D6 GasTurb model, the engine deck was successfully input into the FLOPS model and was able to fly a full multi-drop mission. Conversely, the model derived from the Allison T56 was unable to successfully complete the mission, and failed during its dash to cruise after the first drop. This failure indicates, as suspected, that the raw power carried within the T56 is unable to achieve the required dash speed to return to cruise. As such, the eventual engine configuration converged upon was the Europrop TP400-D6.

6.2. Engine Performance

Through existing engine and aircraft analysis, as well as the use of textbook and software methods, the final engine chosen for use on the SB-22 was the Europrop TP400-D6. Figure 16

below depicts a schematic of the engine developed by Europrop which highlights the various modules developed by different parties which were combined into the TP400-D6.

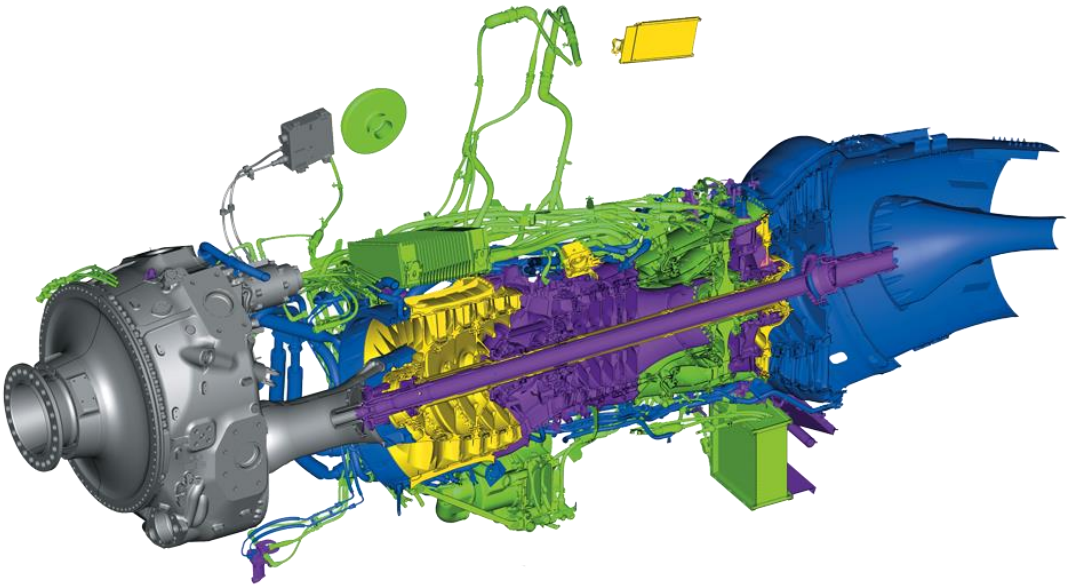

Figure 16. The Europrop TP400-D6, with technology added by Safran in green, Rolls Royce in purple, MTU Aero Engines in yellow, and ITP Aero in blue (Europrop International, n.d.).

This figure emphasizes the modularity of the engine, which adds ease of maintenance through the separability of the various components. Moreover, should certain components become outdated and superior models are designed, these can theoretically be integrated into the current engine framework with minimal difficulty.

In terms of calculating the engine performance, a detailed single cycle analysis was conducted in GasTurb, which produced the following T-s and p-V diagrams depicted in figures 17 and 18, respectively, below.

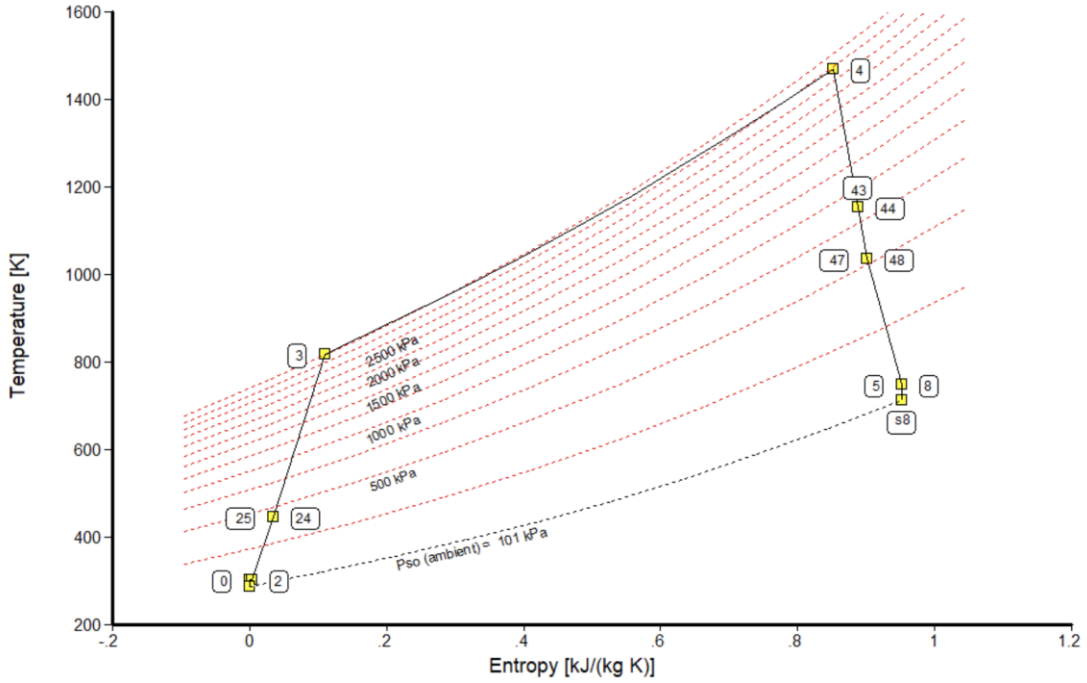

Figure 17. Temperature versus entropy for the Europrop TP400-D6 at takeoff developed using GasTurb.

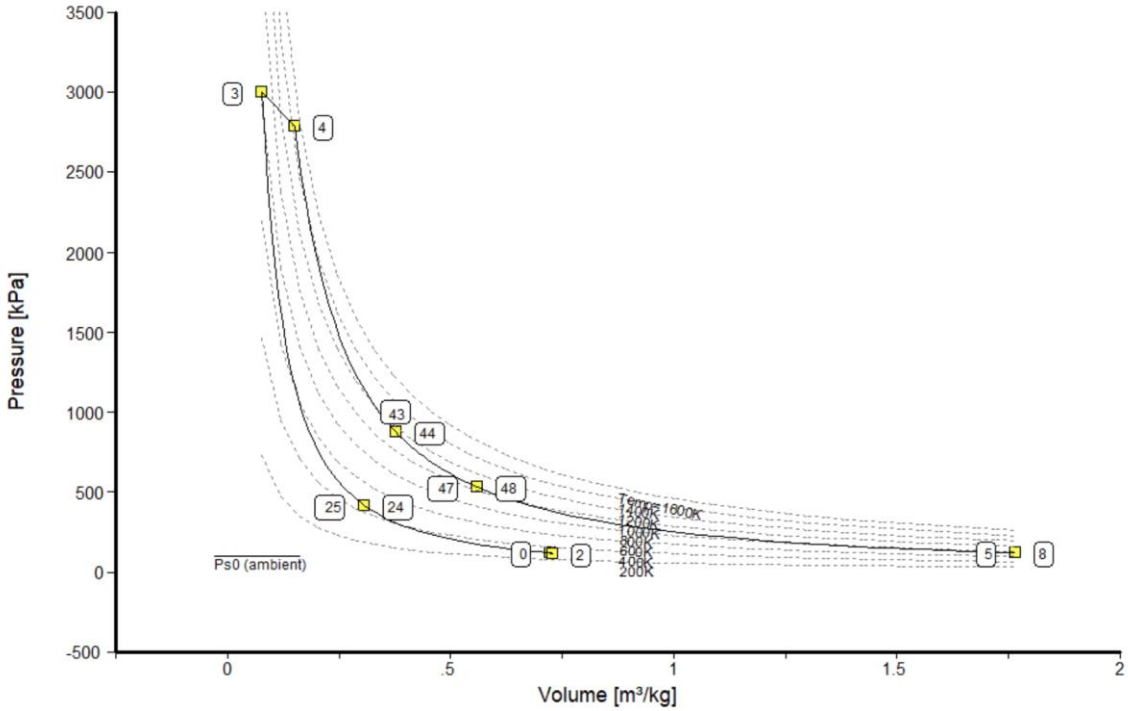

Figure 18. Pressure versus volume for the Europrop TP400-D6 at takeoff developed using GasTurb.

At the compressor exit, stage 3, the flow reaches a maximum pressure of approximately 435 psi (3000 kPa). Stages 4 through 48 represent the different stages of the turbine, going from combustor exit to the high pressure, then intermediate pressure, and lastly low pressure turbines. The flow then exits the nozzle and merges with the external flow, returning to the ambient pressure isobar.

6.3. Engine Placement

In order to determine the optimum placement of the selected engine, rather than set up and solve intense computational simulations in a CFD solver, previous research on the subject was surveyed. Most relevant to the large tube-and-wing aircraft design was research conducted by Blaesser (2019), who leveraged the high power systems available at NASA to develop a comprehensive visualization of the flow around an engine nacelle at different locations along the wing (p. 8).

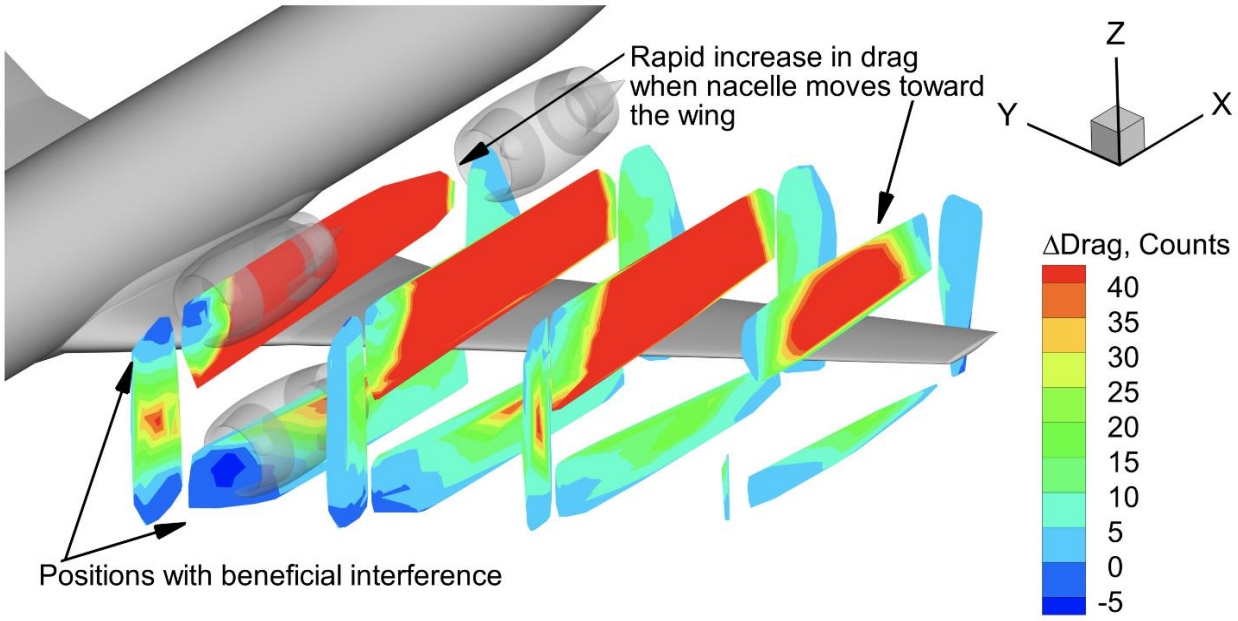

Figure 19. Computational visualization of change in drag for different placements of engine nacelle (Blaesser, 2019, p. 65).

Figure 19 shows the drag experienced by the engine nacelle at different slices along the length of the wing, both above and below the wing surface. At every slice, it can be seen that the engine placed above the wing experiences significantly more drag than the engine below the wing. The best placement is below the wing, slightly ahead of the leading edge, and near the wing root. From this research, it was determined that both engines would be placed beneath the wing, with one closer to the wing root and the other along the length of the wing. These would be relatively centrally placed in order to foster structural stability in the wing-engine system.

6.4. Propeller Design

The propeller configuration typically mounted on the TP400-D6 is developed by Ratier-Figeac (n.d.), and features eight scimitar-shaped, variable pitch blades at a total diameter of approximately 17.5 feet. The blades are composed of a carbon spar enclosed in a composite shell, weighing in at 1,444 lb. The propeller can be operated at four different rotational speed settings (in RPM): 655 for low altitude cruise, 730 for standard cruise, 842 for takeoff, and 860 for special maneuvers. These settings can be slightly tweaked so that the ideal rotational speeds for each of the maneuvers within the flight envelope are accounted for.

An interesting alternative design to the propeller system is the implementation of counter-rotating blades. A counter-rotating design offers a large benefit in propeller efficiency by recovering about 60% of the rotational energy lost in the slipstream of the propeller motion. Figure 20 on the next page compares the impact of dual and single rotation propellers on power correction factor. Given an initial approximation for total activity factor of 800-900, there is a significantly larger power correction factor for the dual rotation propeller, meaning that the propeller is deriving substantially more power by this simple recovery of lost energy.

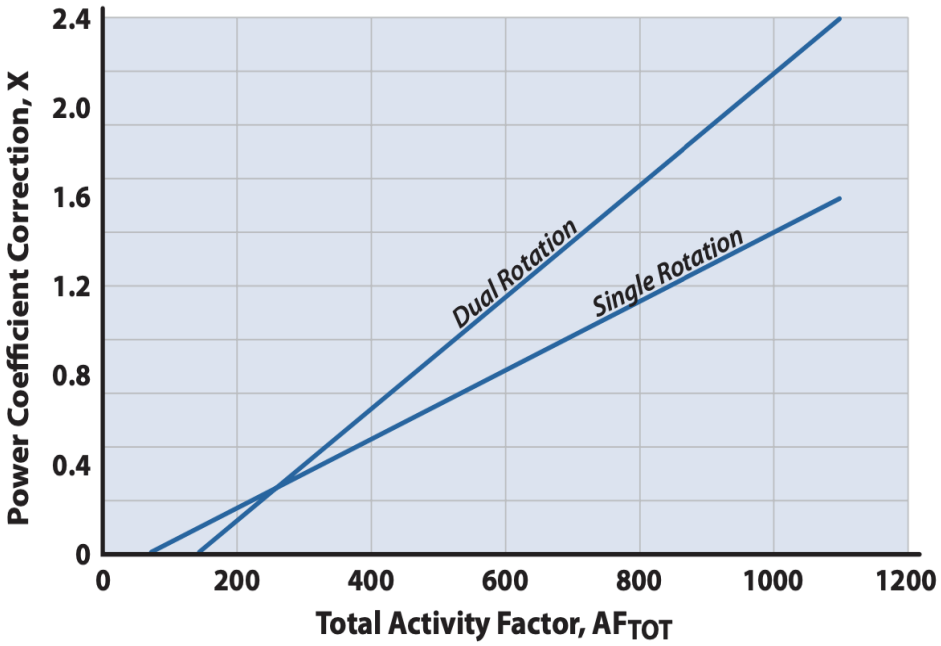

Figure 20. Power correction coefficient versus total activity factor for dual and single rotation propeller configurations (Nicolai, 2010, p. 459).

Unfortunately, the tradeoff for this additional efficiency is an increase in design weight, cost, and complexity. Firstly, to fit on the longitudinal axis two sets of propellers rotating in opposing direction necessitates a larger, more structurally sound, and thus heavier configuration. Multiplying this factor by the 4 engines placed beneath the wings of the aircraft means this will be a significant increase in weight, which will need to be accounted for elsewhere to maintain force equilibrium in the aircraft. As such, as will be illuminated more clearly in section 15, cost is directly proportional to weight, and would thus also increase with the counter-rotating configuration. Lastly, the complexity and time required to achieve a successful counter-rotating configuration is a further barrier to adopting this design.

6.5. Fuel Refinement

Reinforcing the modularity of the engine design, the TP400-D6 is capable of running on several types of jet fuel, including Jet A, Jet A1, Jet B, JP4, JP5, and JP8. In order to create an informed decision on the kind of fuel that will actually be used by the aircraft, a GasTurb model was developed for the engine configuration using several fuel types which were available within the software package. These options include the generic GasTurb fuel, which closely resembles Jet A, JP4, JP10, natural gas, and hydrogen fuel.

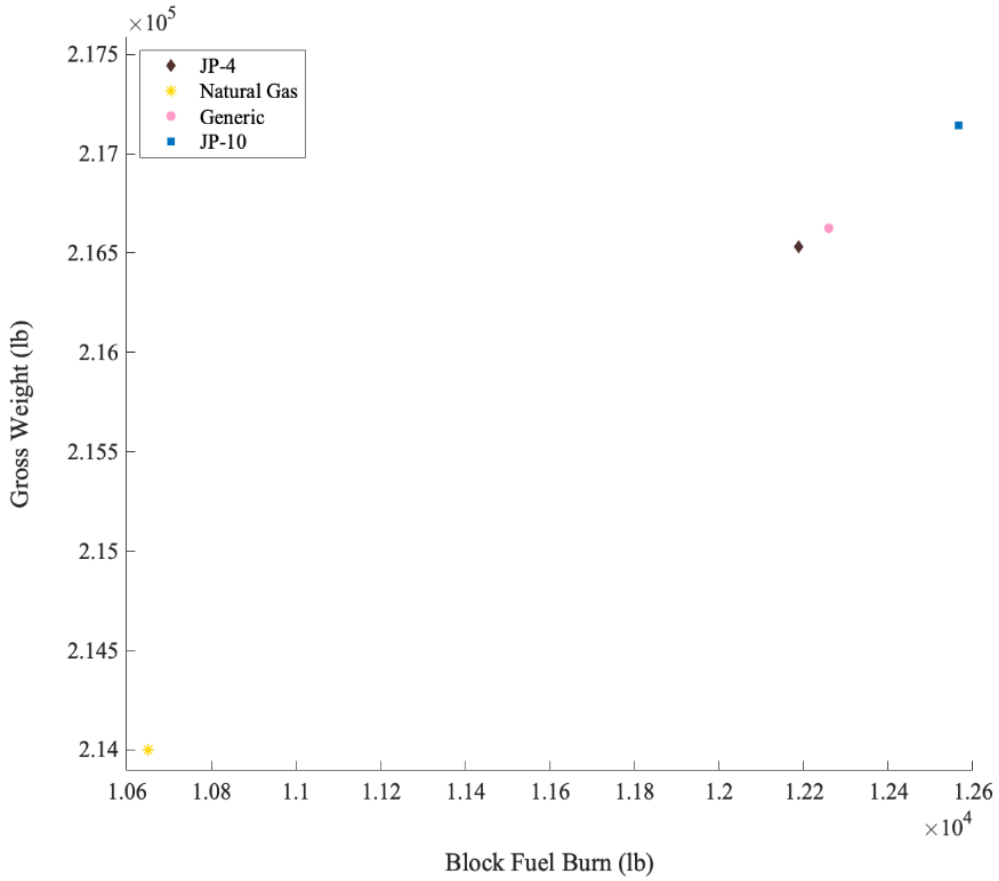

Figure 21. Takeoff gross weight and block fuel burn graphed for four successful fuel configurations derived from GasTurb.

Figure 21 compares the FLOPS output for gross weight and block fuel burn for the fuel configurations which were successfully able to complete the mission. Hydrogen fuel failed, and due to its incompatibility with the engine configuration anyway, no further work was done in order to explore how hydrogen fuel could be incorporated into the propulsion design. Natural gas is also currently incompatible with our engine as it is configured, however FLOPS was able to successfully complete a theoretical mission with it as fuel, so it was included in this comparison. Incidentally, natural gas also was by far the best fuel source in terms of block fuel burn and gross weight; however, JP-4, the next-best alternative, was the fuel source chosen for our design. This decision was made on the basis of practicality. First, as just mentioned, the fuel has no history of use with the TP400 D-6, meaning it is likely that incorporation of natural gas in the propulsion system design would necessitate large changes to the engine itself. Moreover, in order to keep natural gas in its liquid state for use as fuel, the substance must be kept at supercooled temperatures. As such, additional systems for cooling must be incorporated into the calculation for fuselage weight, space in the wing must be made in order to hold these systems, and a waterfall of subsequent complications must be accounted for in the design. There is also very little research into or existing natural gas aircraft configurations, meaning the technology is still in its infancy, and would likely not be ready for the required 2030 entry into service.

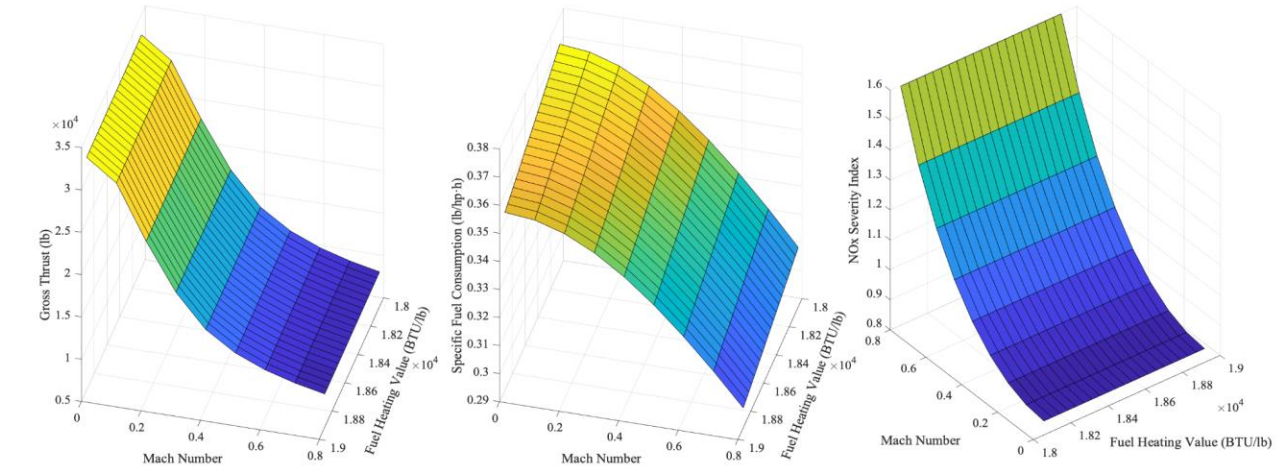

Figure 22. Gross thrust, SFC, and NOx severity index compared for different fuel heating values at various Mach numbers

Furthermore, in order to achieve a more holistic understanding on the effect of fuel type on aircraft performance, a parametric study was conducted in GasTurb comparing gross thrust, SFC, and NOx severity index for an array of fuel heating values at different Mach numbers (Figure 22). The resulting analysis showed most notably that as fuel heating value increases, there is a noteworthy decrease in SFC. As such, researchers considered alternative jet fuels with slightly lower fuel heating values than JP-4 like JP-8. However, the main obstacle in their acceptance was the inability to develop a sufficiently accurate computational study of JP-8 due to the limitations of GasTurb. Without having the actual fuel embedded in the GasTurb program, it cannot be simply assumed that JP-8 can be modeled as JP-4 with a lower fuel heating value. There are additional complexities in the chemical makeup of engine fuel that are not captured, and how significant these discrepancies in reality and the GasTurb model can not be adequately defined. Thus, the final result of this exploration was the use of JP-4 as the fuel source for the SB-22.

7. Aerodynamics

7.1. Lift Analysis

The aerodynamic lift for the aircraft was calculated for steady and level flight conditions, which is the cruise configuration with flaps fully retracted. To analyze the lift characteristics of the aircraft, an empirical method described in *Elements of Preliminary Aircraft Design* by Schaufele and VSPAERO, a vortex lattice solver developed by NASA, were utilized. The methods described by Schaufele were used to produce low speed lift curves based off of airfoil and wing planform parameters (Schaufele, 2007). To do so, an airplane lift curve slope was determined based on the wing aspect ratio (AR) and sweep angle. The cruise configuration curve was constructed based on CL_{cruise} at $(L/D)_{max}$ found from VSPAERO and CL_{max} for the cruise curve was determined from airfoil section Cl_{max} and airfoil thickness-chord ratio trends. From there, the takeoff and landing low speed lift curves were generated by shifting the zero lift angle of the cruise curve based on wing sweep angle, flap deflection angle, and flap size. The lift curve slope for each configuration is shown in Figure 23 and a summary of CL_{max} is shown in Table 8.

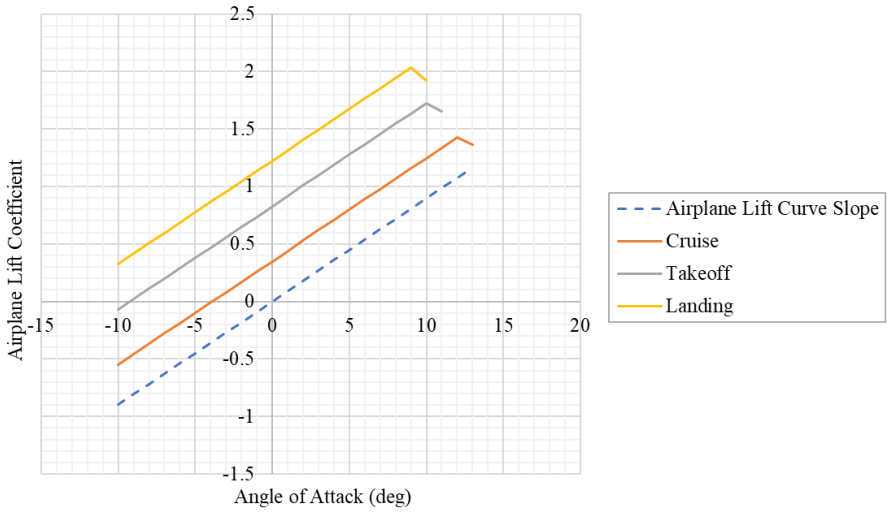

Figure 23. Low Speed Lift Curves

According to Schaufele, the typical deflection angles for takeoff and landing are 15°-25° and 40°-50°, respectively. The maximum deflection angle values were chosen for each configuration to ensure the aircraft met stall and payload drop characteristics.

Table 8. CL_{max} Values

Configuration	CL,max
Cruise	1.43
Takeoff	1.72
Landing	2.03

7.2. Drag Analysis

The drag analysis for the aircraft was carried out in VSPAERO, which has a Parasitic Drag Tool that uses existing geometry from OpenVSP, equations for friction coefficient C_f, form factor equations, and defined flow conditions to calculate the full parasitic drag build up (OpenVSP, n.d.). The analysis involves the wetted area of all components in the OpenVSP model: the wing, fuselage, horizontal stabilizer, vertical stabilizer, engine nacelles, and engine pylons. The default settings and equations were used in the VSPAERO parasitic drag analysis; this includes the Blasius Laminar C_f Equation, Schlichting Compressible Turbulent C_f Equation, Hoerner Form Factor Equation, and Hoerner Streamlined Body Equation. The parasitic drag, CD_0, was analyzed for cruise conditions and the total build up is shown in Figure 24 and Table 9.

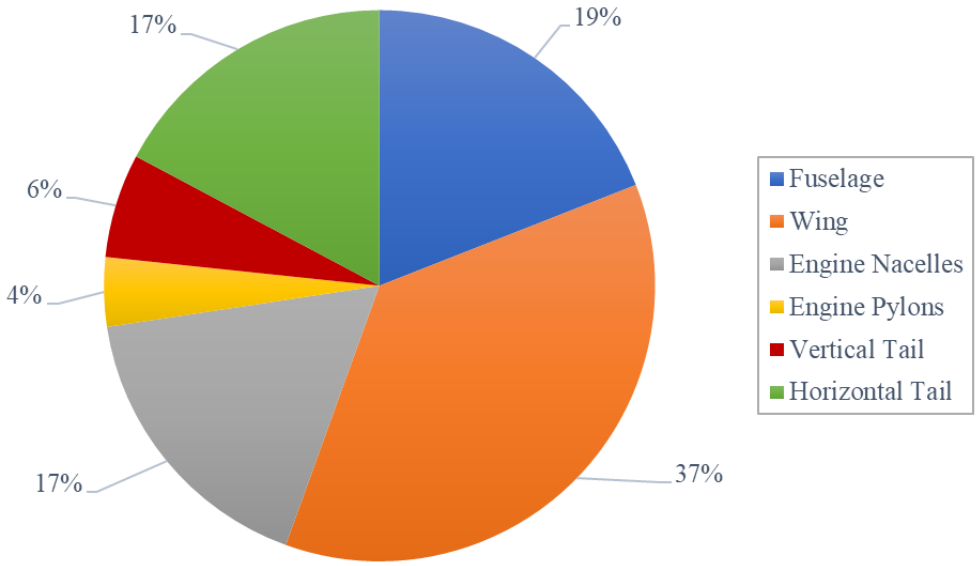

Figure 24. Parasitic Drag Build Up in Cruise

Table 9. Parasitic Drag Values in Cruise

Components	CD,0	% Contribution
Fuselage	0.00300	19.04
Wing	0.00575	36.48
Engine Nacelles	0.00269	17.09
Engine Pylons	0.00064	4.06
Vertical Tail	0.00096	6.11
Horizontal Tail	0.00271	17.23
Total	0.01576	100

A lift-to-drag ratio curve was generated from a VSPAERO simulation to determine $(L/D)_{max}$ and the corresponding CL_{cruise} and angle of attack (AOA). The aircraft has an $(L/D)_{max}$ of about 17.7 for a CL_{cruise} of 0.62, as shown in Figure 25. This CL_{cruise} has the aircraft cruising at an AoA of 3°.

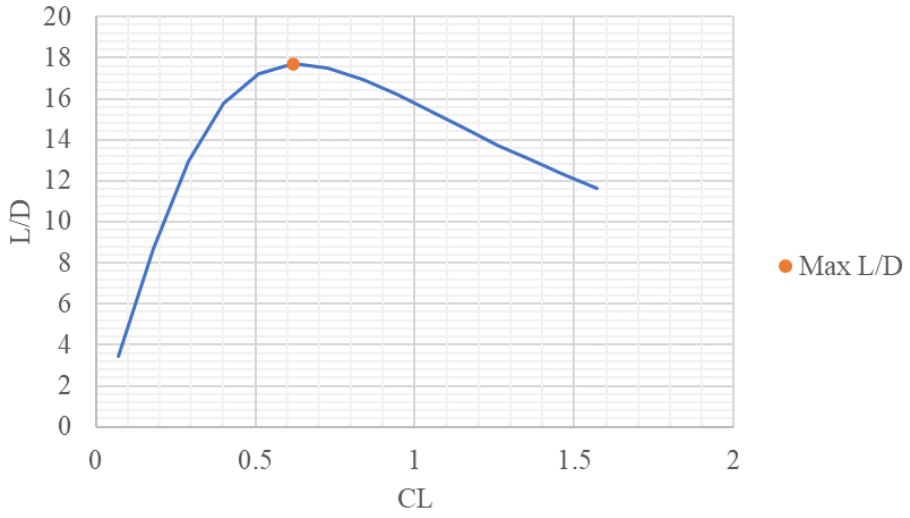

Figure 25. L/D vs. CL in Cruise

The drag polar for the aircraft in cruise is shown in Figure 26. The plot highlights $(L/D)_{max}$ where CL_{cruise} is 0.62 and the total drag CD is 0.04.

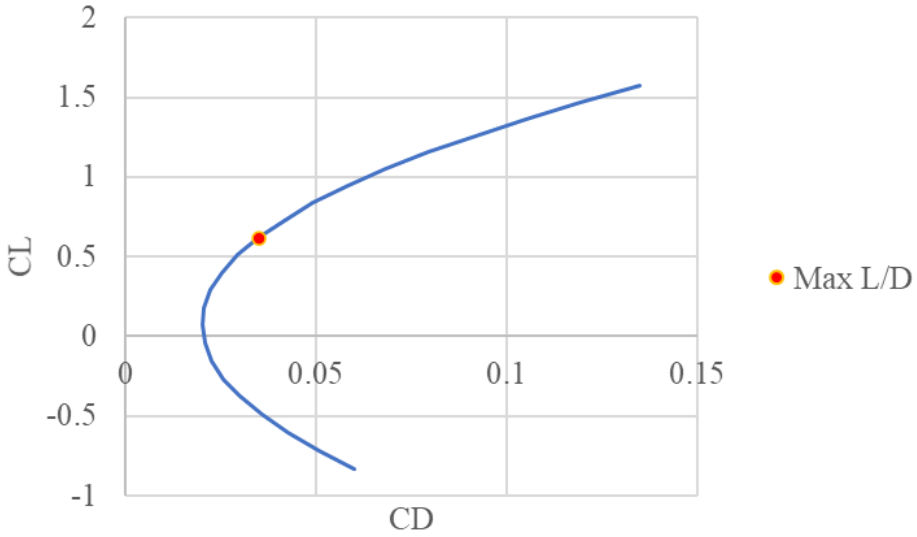

Figure 26. Drag Polar in Cruise

7.3. Airfoil Selection

When selecting the airfoil for SB-22, five different NACA airfoils were studied using the VSPAero aerodynamic software within OpenVSP. The aerodynamic characteristics used to investigate each airfoil were the maximum coefficient of lift, the coefficient of lift when AoA is 0°, the coefficient of drag when AoA is 0°, the lift to drag ratio (L/D), and the thickness to chord length ratio (t/c).

Table 10. Airfoil Trade Study

Parameters	NACA 1412	NACA 2412	NACA 4415	NACA 63008	NACA 63010
CL,max	**1.45**	**1.45**	1.43	1.06	1.37
CL,0	0.172	0.178	**0.191**	0.165	0.165
Cd,0	**0.00088**	0.00101	0.00139	0.0016	0.000941
L/D Ratio	~17.3	~17.2	**~17.7**	~16.3	~17.1
T/C Ratio	0.12	0.12	**0.15**	0.08	0.1

The results in Table 10 show that the NACA 2412 airfoil and NACA 1412 airfoil have the highest maximum coefficient of lift values of 1.45. The NACA 1412 also has the lowest coefficient of drag when AoA is 0°, making it a solid option. However, the NACA 4415 airfoil was chosen due to its competitiveness in each category investigated in the trade study, and having the highest thickness of 15%. The NACA 4415 airfoil has a maximum coefficient of 1.43, which is not too far behind the highest values of 1.45. Its high lift to drag ratio in comparison to other airfoils made the decision to choose the NACA 4415 easy.

7.4. Wing Configuration

In designing our wing, we used our TOGW of 216,355 lb and our wing loading value of 85.70 to size the area of our wing to be 2525 square feet. The wing is located 35 feet along the fuselage with a wingspan of 145 feet. The average chord is 20.88 feet, giving the wing an AR of roughly 8.3.

The wing was tapered to improve aerodynamic efficiency. The wing was split into four different sections, each having different varying root chord and tip chord lengths (with the root chord length being larger). Because the highest moment tends to be concentrated at the wing root, the taper will make this area wider and thicker – which is good for a plane that requires high load situations like aerial firefighting. The wing was also given a 0.5° anhedral due to its high placement and to achieve desired roll stability characteristics.

7.5. Empennage Configuration

In designing our empennage, both the horizontal and vertical configurations had to be sized. The main objective of the empennage was to meet the FAA CFR Part 25 stability requirements. To start with, the initial sizing of the empennage was conducted with the tail volume coefficient method. The horizontal tail volume coefficient, C_{HT}, and the vertical tail volume coefficient, C_{VT}, for the Lockheed C-130 were used as a starting point; C_{HT} and C_{VT} were 0.94 and 0.053, respectively (Nicolai & Carichner, 2010). Changes in the empennage configuration can greatly affect the stability, so the horizontal and vertical stabilizers were sized accordingly and stability calculations were conducted in VSPAERO.

A trade study was carried out for the empennage configuration, with stability being the most important characteristic, as seen in Table 11. The T-tail design was chosen due to its high aerodynamic efficiency and positive impacts on stability. These are areas in which the SB-22 "Woodzy Owl" was originally lacking. However, a 3 foot cruciform from the top of the vertical tail was given to the horizontal tail. There is more structural support within the tail with a slight cruciform rather than no cruciform – which can be seen with a lot of existing designs that implement T-tails.

Table 11. Empennage Configuration Trade Study

Type	Weight of Importance	T-tail	Cruciform	Conventional
Cost	2	1	2	3
Stability	4	3	2	1
Weight	2	1	2	3
Space for Cargo	1	3	2	1
Total	-	19	18	17

The vertical stabilizer has an area of 256 square feet and sweep of 45 degrees, and a projected span of 22.1 feet. It is split into two different sections, both having varying tip and chord lengths. The horizontal stabilizer was aimed to have an AR of about half of the AR of the main wing, which was sized to be 4.38. To match the stability requirements (to be later discussed), the horizontal stabilizer was given a span of 71.2 feet and a chord length of 16.3 feet. The NACA 0010 airfoil was chosen for both the vertical and horizontal stabilizers. A symmetrical airfoil is required to maintain stability characteristics and a thickness less than the main wing will prevent stalling of the stabilizers before the wing. The horizontal stabilizer was given no incidence angle, as the desired trim angle of 3 degrees was already reached without the incidence angle.

7.6. High Lift System

To achieve the required amount of lift for landing and takeoff, trailing edge flaps were implemented into the wing design. The trailing edge flaps will be deflected by 25° and 50° for takeoff and landing, respectively. The sizing of the flaps follows methods from Raymer's textbook and are dependent on the sizing of the ailerons, which will be discussed in detail in the control surface design section. The dimensions for the trailing edge flaps are shown in Table 12.

Table 12. Flap Parameters

Parameter	Value
Flap Span (ft)	32
Flapped Area (ft^2)	1282
Chord (ft)	5.22
Chord Ratio	0.25

7.7. Control Surface Design

The sizing of the control surfaces were based on historical data and recommendations by Raymer (Raymer, 1992). These control surfaces include ailerons, elevators, and a rudder so the aircraft is able to maintain its roll, pitch, and yaw characteristics throughout the flight. According to Raymer, aileron chords are typically 25% of the wing. It was decided that the aileron span should be minimized within the historical data trend to allow as much room as possible for the flaps in order to generate as much lift as possible to meet performance requirements. The total aileron span boundary is depicted by the horizontal red lines in Figure 27. As such, the aileron spans 35% of one wing, the flaps span 55%, and the remaining 10% of the span are normal wing surfaces.

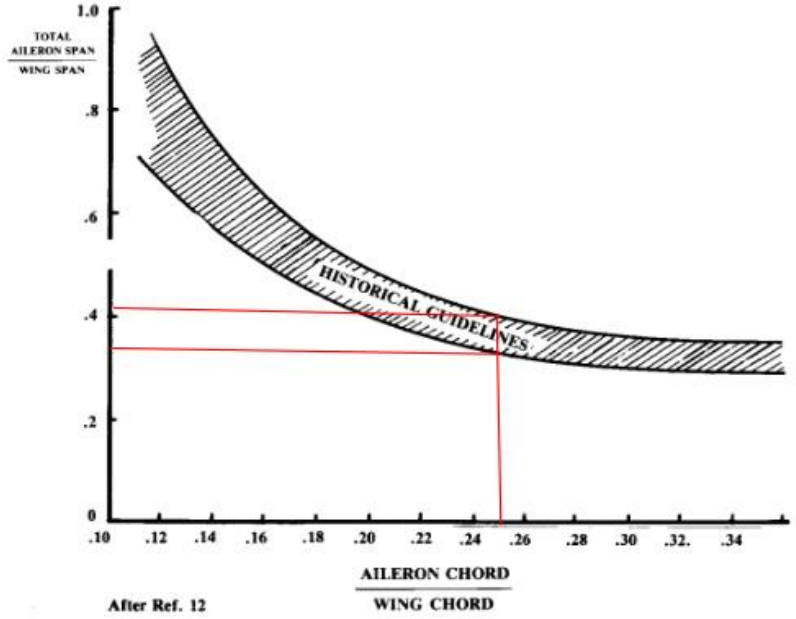

Figure 27. Historical aileron sizing trends (Raymer).

The rudder and elevators have chords that are 30% of their respective empennage surfaces. As for the span, elevators and rudders typically span about 90% of the vertical and horizontal tail spans, respectively (Raymer, 1992). Control surface parameters are summarized in Table 13.

Table 13. Control Surface Parameters

Parameter	Aileron	Elevator	Rudder
Span (ft)	20	32	19
Span Ratio	0.35	0.90	0.90
Chord (ft)	5.22	4.89	6.96
Chord Ratio	0.25	0.30	0.30

8. Stability and Control

Stability was an important factor to consider when sizing areas of the SB-22. To be sure SB-22 was a sufficiently stable design, three stability parameters were tested – longitudinal static stability (pitching stability), lateral static stability (rolling stability), and directional stability (yaw stability). Each of these plots were generated from VSPAERO with a center of gravity located at 49.14 ft along the x-axis from the nose of the aircraft while assuming full payload. However, due to the aircraft having differing levels of payload throughout a flight, the center of gravity location will not stay consistent throughout flight. During initial analyses prior to finalizing C.G. location, each of the stability parameters were tested with success using differing values of center of gravity between 40 ft and 52 ft. Therefore, the designers have high confidence in the aircraft's stability performance.

8.1 Longitudinal Static Stability

Longitudinal static stability was the first stability parameter that was met during aircraft sizing. For an aircraft to be longitudinally stable, the value of CM_y, the pitch moment coefficient, at AoA (α) = 0 must be positive, and the slope of CM_y with respect to α must be negative. The longitudinal stability graph and stability derivative was calculated using VSPAERO, with the outputs shown in Figure 28.

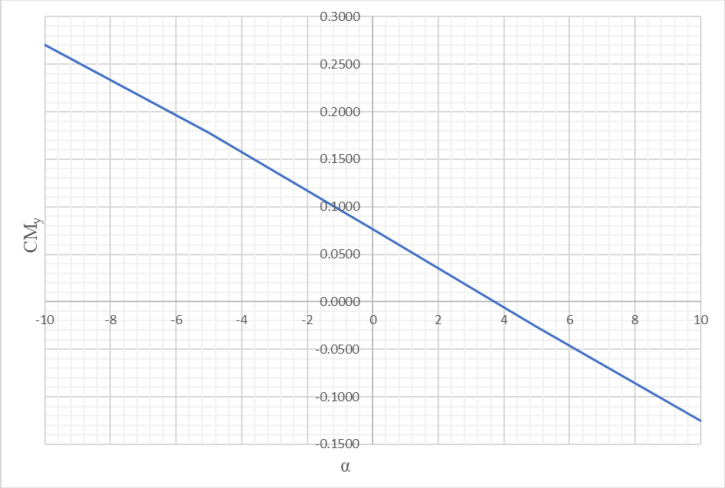

Figure 28. CMy vs. α

The value of CM_y at $\alpha = 0$ is positive, and the slope of CM_y with respect to α is -1.17 – matching the criteria needed for longitudinal stability. The trim angle is approximately 4 degrees, which was the target for our design. Longitudinal stability can also be proven with a positive static margin. The static margin was calculated in OpenVSP to be 0.1939, therefore also making the SB-22 longitudinally stable. Based on the final C.G. of 49.14 ft, the neutral point is located at 53.99 ft, as shown in Figure 29.

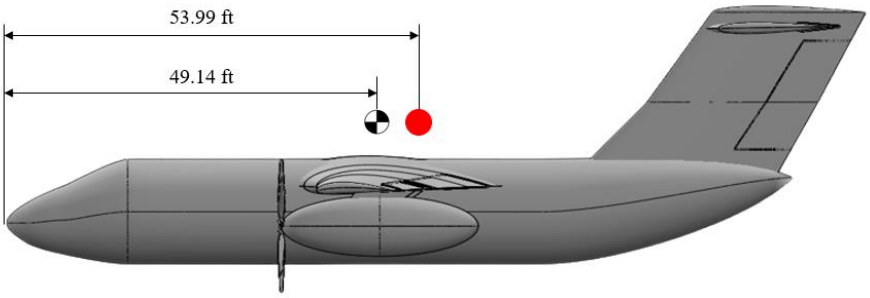

Figure 29. C.G. and Neutral Point Location

8.2 Lateral Static Stability

For lateral static stability, the slope of CM_x, the roll moment coefficient, with respect to sideslip angle β must be negative. The value of the slope was calculated to be -0.0406.

Therefore, the aircraft has lateral static stability, as shown in Figure 30. It should be noted that the data output for lateral stability from VSPAERO is flipped; this means the plot below does indeed show lateral stability.

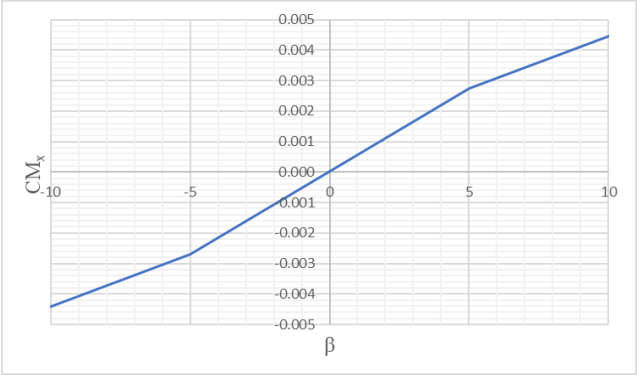

Figure 30. CMx vs. β

8.3. Directional Stability

For directional stability, the slope of CM_z, the yaw moment coefficient, with respect to β must be positive. The value of the slope was calculated to be 0.0381. Therefore, the aircraft has directional stability, as seen in Figure 31. It should be noted that the data output for directional stability from VSPAERO is flipped, similar to lateral stability. This means the plot below does indeed show directional stability.

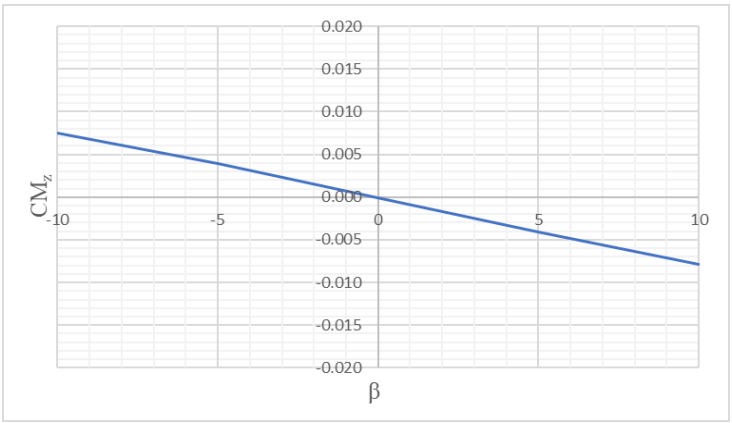

Figure 31. CMz vs. β

9. Structures and Loads

9.1. Fuselage

The fuselage is composed of evenly spaced frames and longerons, a skin, and bulkheads located at high stress locations and discontinuities. The bulkheads are located at the wing-fuselage joints, empennage-fuselage joint, landing gear-fuselage joint, and the fire retardant tank drop door to provide more robust strength in comparison to the thinner frames. The frames and bulkheads are spaced 20 inches apart to allow for a balance of bending strength and weight. The longerons are spaced 4 inches apart to minimize buckling of the fuselage skin to evenly distribute loads from the skin to the frames and bulkheads. The tubular shape of the fuselage allows for even pressure distribution along the skin surface of the fuselage. A composite, semi-monocoque fuselage was considered but an aluminum skin was selected since carbon fiber reinforced composite (CFRP) fuselage skin is still costly and has not achieved widespread use in the aviation industry yet. CFRP does offer a significantly lighter and more fatigue resistant alternative to its metal counterparts although fatigue from the high cyclical loads is difficult to inspect and quantify. The dimensioning of the fuselage components are to be further optimized using FEA bending analysis and buckling analysis. The frames and longerons are made of 7075-T6 aluminum and the skin is made of 2024-T3 aluminum to offer high strength at a lower weight than its steel counterparts. Towards the rear section of the fuselage an access door is situated to allow ease of access into the cargo bay. The door drops vertically to create a ramp onto the cargo floor, and has integrated rollers along both the door and cargo floor to allow for easier loading and unloading. This floor also allows for easier inspection of the payload and its systems.

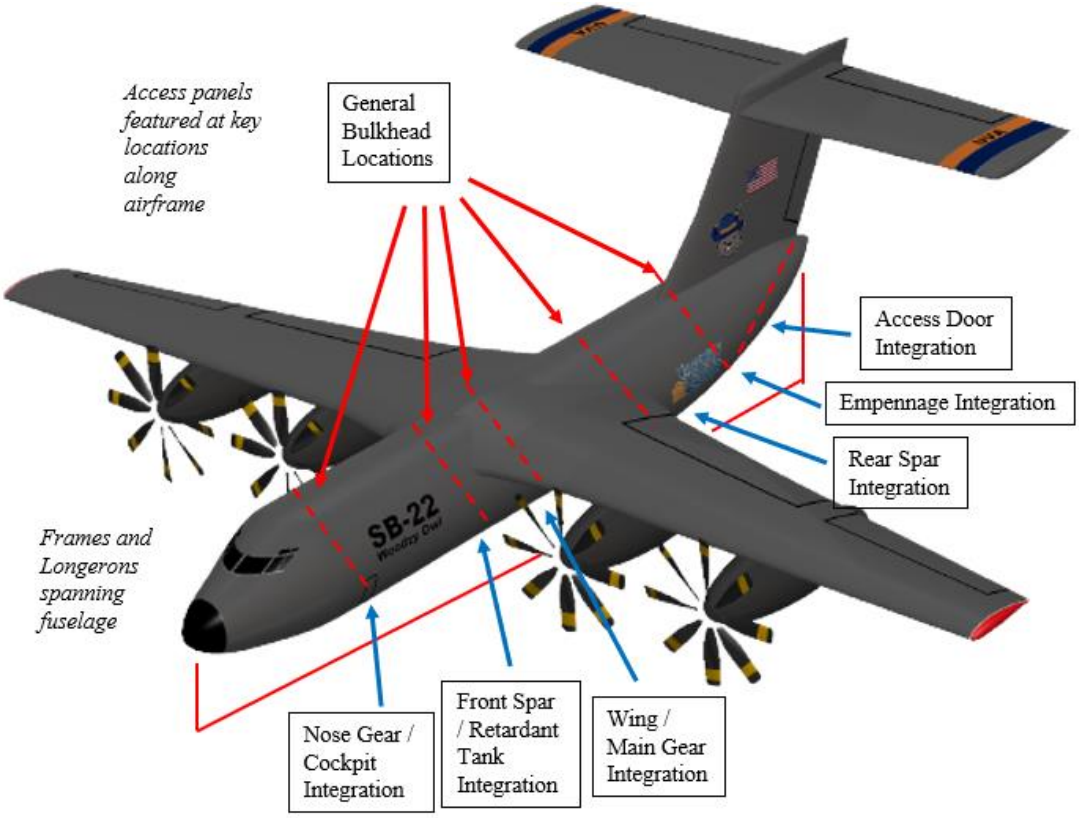

Figure 32. Fuselage Structure Highlights

9.2. Wing

The structural analysis of the wing structure began with the V-n diagram combined envelope following the Federal Aviation Regulations Part 25 guidelines. Following FAR Part 25, the design speeds for maneuvering, diving, cruising, stall and maximum gust intensities were calculated and plotted against the load factors. As specified in FAR Part 25, the load factors range from -1 to 2.5. The diagram was constructed using a gross weight of 216,355 lbf and a cruise Mach number of 0.45 at cruise altitude of 33,000 ft. The speeds represented in the V-n diagram are in units of knots equivalent airspeed (KEAS) in consideration of the change of density along the change in altitudes from sea level to cruise level. The gust lines were constructed following FAR Part 25 guidelines with reference gust velocity spanning from 56 ft/s

EAS at sea level to 20.86 ft/s EAS at 60,000 ft. The V-n diagram shows that the aircraft is able to safely exceed dash speed of 300 knots at 30,000 ft as specified by the RFP.

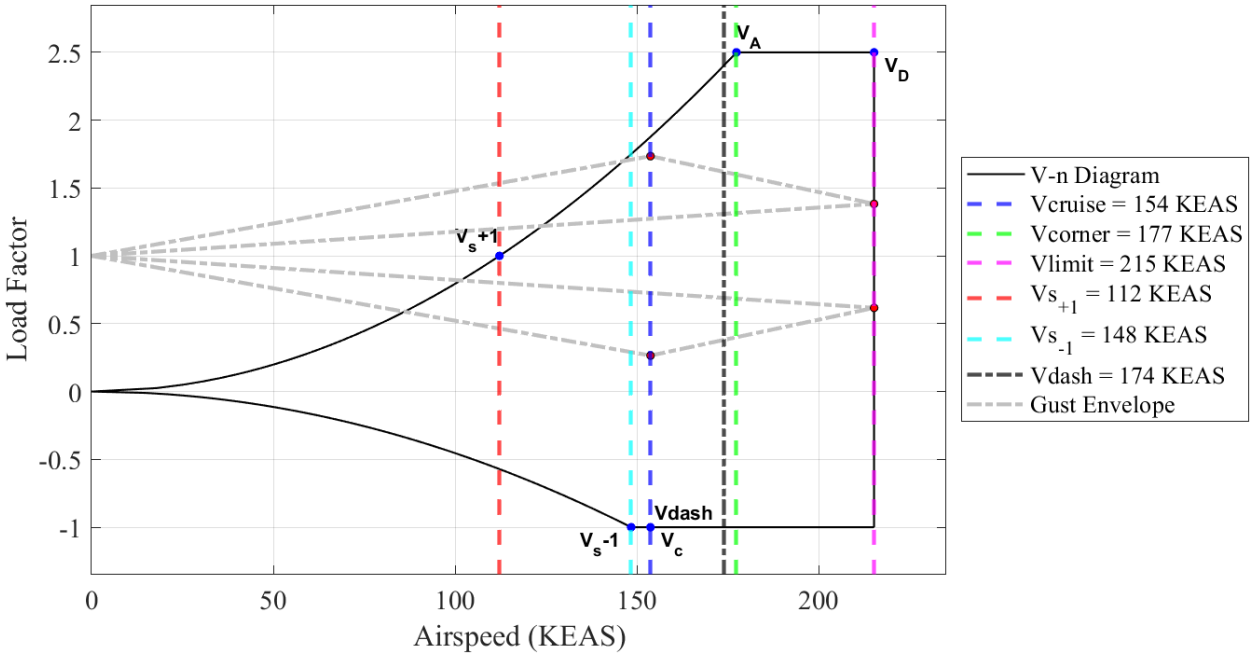

Figure 33. V-n Diagram Combined Envelope

A lift coefficient distribution profile was obtained from VSPAERO for the half span of the wing and imported into MATLAB. The lift coefficient profile was translated into a lift load distribution profile using dynamic pressure and local chord lengths. Using the methods specified in Bruhn's book, the shear and bending moment diagrams for the wing were constructed in MATLAB. At the wing root, the wing experiences 205,784 lbs of shear loading and a bending moment of 30,780,200 lbs-in at the most extreme flight condition of 2.5 load factor. A safety factor of 1.5 was used to size the wing spars and ribs.

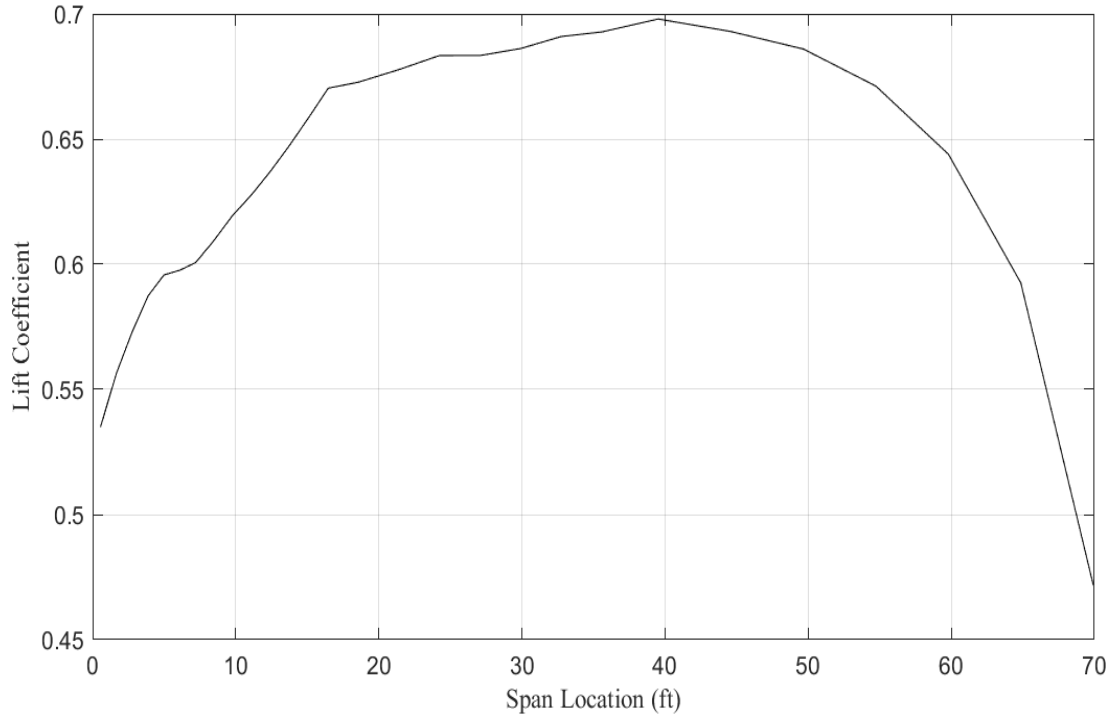

Figure 34. Wing Lift Coefficient Distribution Profile

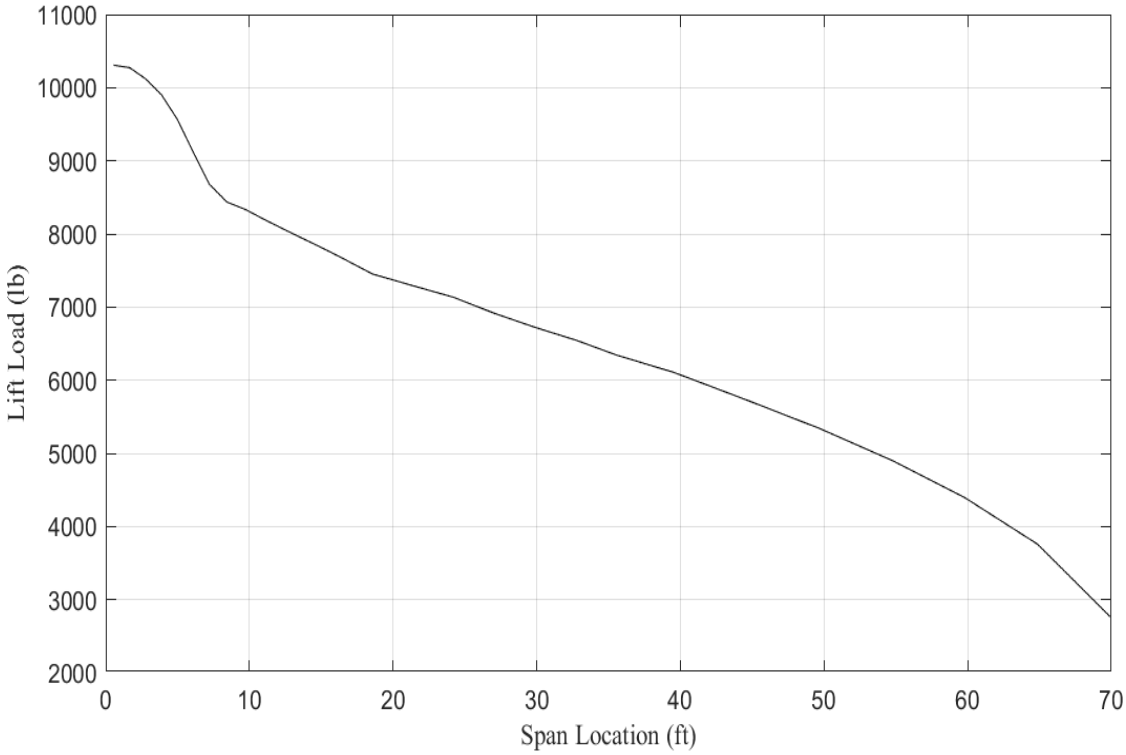

Figure 35. Wing Lift Load Distribution Profile

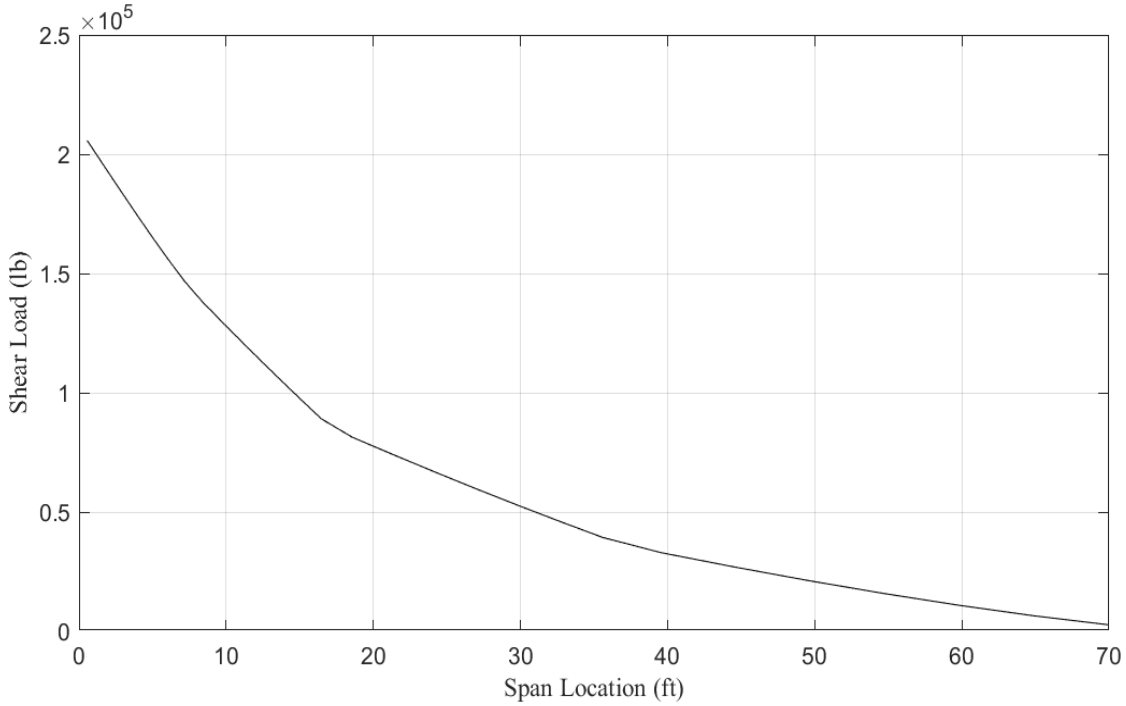

Figure 36. Wing Shear Load Distribution Profile

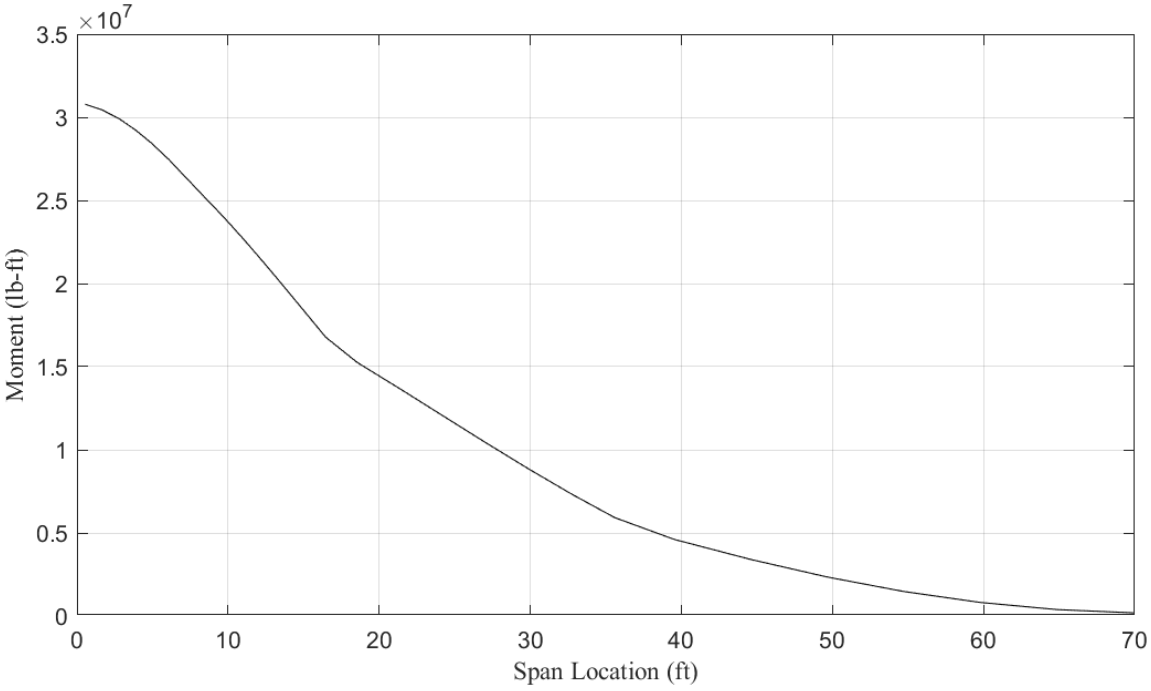

Figure 37. Moment Distribution Profile

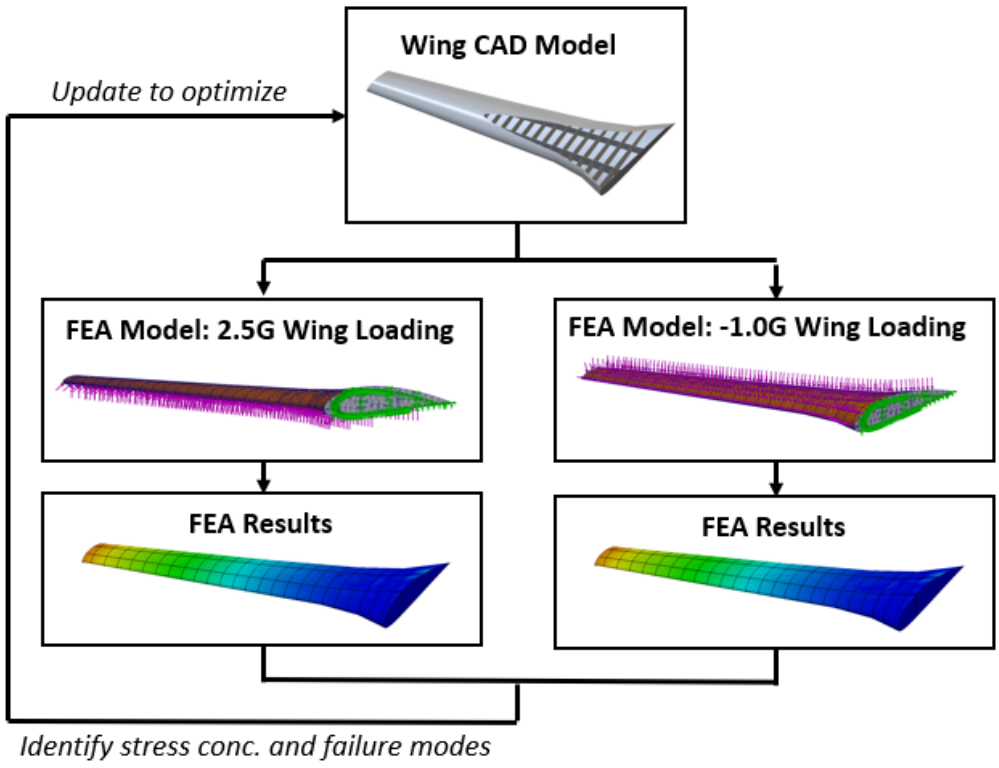

Figure 38. Wing CAD / FEA Iteration Loop

The wing model was optimized using an interactive process in which the wing was recursively loaded using both the 2.5 and -1 load factors in an FEA model and resized to meet strength requirements, similar to the depiction in Figure 38 above. Local failure points and stresses were related to materials properties to down select both dimensions and materials selection. Aeroelastic, fatigue, and buckling analysis may be utilized to further optimize and analyze the structure.

The wing structure consists of stringers, ribs, spars, and a skin. The ribs are spaced with 30 inches intervals to allow a balance of strength and minimized weight. The stringers are spaced with 4 inch intervals to minimize buckling of the skin. The ribs are 0.5 inches thick and the spars are 1 inches thick. The skin is 0.1 inches thick. The ribs, spars, and stringers are made of 2075-T6 aluminum for added strength and fatigue resistance without sacrificing a significant loss in

stiffness. The skin of the wing is made of 7178-T76511 aluminum for its excellent stiffness, mechanical strength, and fatigue resistance as it will aid in reducing buckling and fracture. The aluminum alloys also exhibit good corrosion resistance. The materials considered for selection and their material properties are summarized in Table 14.

Table 14. Materials Selection

Material	Endurance Limit (psi)	Youngs Modulus (psi)	Yield Strength (psi)	Ultimate Strength (psi)	Shear Strength (psi)	Density (lb/in^3)
Al 7075-T6	23,000	10,400,000	73,000	83,000	48,000	0.102
Al 2024-T3	20,000	10,600,000	50,000	70,000	41,000	0.100
Al 7050-T7451	-	10,400,000	68,000	76,000	44,000	0.102
Al 7178-T76511	30,000	11,603,000	75,000	85,000	50,000	0.1018
Al 7055-T77511	-	-	82,000	86,000	-	0.103
Al 6061-T6	14,000	10,000,000	40,000	45,000	30,000	0.0975

9.3 Empennage

The empennage is also similar in wing structure with the use of spars and ribs. Because the aspect ratio of the vertical and horizontal surfaces is lower than that of the wing, the bending moments are significantly smaller and much of the empennage structure is dedicated to handling the loads at and near the control surfaces, specifically the elevator and rudder. Because the horizontal stabilizer is mounted near the top of the vertical tail, the T tail requires higher torsional stiffness requirements to minimize flutter effects. Towards the tip, the T tail must be designed for twice the relative torsional stiffness compared to conventional tail. Thus, torsional and aeroelastic analysis will be utilized to size the internal components of the empennage and the horizontal-vertical tail junction so that torsional stiffness requirements are met.

9.4. Landing Gear

The landing gear absorbs the static loads of the aircraft and the dynamic loading upon landing. Additionally, the landing gear is the primary ground control mechanism. The loads are absorbed using oleo struts with gas-oil hydraulic shock absorbing chambers and hydraulic

brakes. The landing gear is vertically retracted into the fuselage using vertical guiding tracks. The vertical retraction system was selected over a folding retraction system to minimize weight and that the fuselage has empty space to accommodate a vertical retraction rail. Folding retraction mechanisms can be used to fit the landing gear into smaller volumes of the airframe at the expense of substantial weight increase. Landing gear pods are not featured as the aircraft is designed for aerial firefighting as opposed to utility aircraft mission profiles such as C-17 and C-130 in which freeing up fuselage space was a driving factor. Although the oleo struts absorb the majority of the landing loads, the attachment mechanism to the fuselage allows direct transmission of loads into the airframe. The landing gear also features an oleo-pneumatic leveling system which allows the aircraft to land on runways that are not completely leveled.

In a tricycle landing gear configuration such as the one featured on the SB-22, there are two main gears attached to the airframe behind the center of gravity that support most of the weight of the entire aircraft (~85% of the entire weight). Each main gear has four wheels to allow the aircraft to safely accommodate the landing loads. The set of two wheels on the nose gear provide a level of steering control. There are three main advantages to the tricycle configuration that are advantageous for the firefighting mission design. The first is that this configuration allows for a more forceful application of the brakes during landings at high speeds without having the aircraft nose over. In the application of firefighting aircraft which could be forced to land in rural locations on short notice this is a critical design feature of the landing gear. The second advantage is that since the aircraft is more level while taxiing with the tricycle configuration, the pilot has much better visibility during takeoff and landing, again potentially crucial in firefighting applications when smoke may cover the surrounding areas making pilot visibility extremely important in order to successfully takeoff and land. Finally, the tricycle

configuration provides more directional stability during ground operation due to the center of gravity being kept in front of the main wheels of the aircraft, again advantageous for takeoff and landing in sub ideal conditions present in firefighting applications (CFI Notebook, 2022, para. 3).

For the tire selection, a trade was first done to compare the two main aviation tire brands which were Michelin and Goodyear. After a quick dive into each company's reputation in the industry, it was found that Goodyear aircraft landing gear tires hold a significantly higher reputation and command a greater demand. Based on this informal industry survey, the specific Goodyear tires to be used were selected based off of the 2021 Goodyear data sheet for their rated loads. As noted earlier, the nose gear only sees up to about 15% of the entire weight of the aircraft, so the two tires on the nose gear will use Goodyear Type VIII, 36x11 which have a rated load of 26,500 lb. For the two gears mounted to the airframe which will support the majority of the aircraft weight, the selected tires were Goodyear Type VIII, 44x16 which have a rated load of 38,400 lb. Although these tires only feature a rated load about 10,000 lb higher than the nose gear tires, the airframe mounted gears consist of eight wheels in total, meaning a combined rated load of 307,200 lb compared to the nose gear combined rated load of 53,000 lb. This equates to the nose gear being able to handle up to 17.3% of the full weight (close to the estimated 15%), and factors all loads with a 1.5 factor of safety. The chosen tire and landing gear are modeled in 3D on the following page in Figures 39 and 40.

Figure 39. Landing Gear Tire Good Year CAD

Figure 40. Main Gear CAD Model

10. Subsystems

10.1. Fuel System

The aircraft consists of integral fuel tanks between the main spars within each wing. Each fuel tank has a fuel pump to provide consistent fuel flow to the engines and an auxiliary power unit. A gravity fed fuel system was not selected since the aircraft performs a varied set of fire retardant drop maneuvers. Fuel valves are included for each tank so that if one tank is punctured, fuel from the other tank does not drain. The tanks also include a fuel gauge that is displayed in the cockpit to closely monitor fuel consumption during missions. There are fuel doors for each tank with a standard refuel rate of 1000 liters per minute. Using two fuel trucks, depicted on Figure 41, the aircraft can be refueled at a rate of 2000 liters per minute with two fuel hoses flowing simultaneously. Calculated in FLOPS, the aircraft will carry a total of 19,627 lb of fuel based on the mission profile. Each tank will carry 9,814 lb of aircraft fuel with a volume of 1429 gallons. Using the approximate lower-limit density of JP-4 aircraft fuel, the aircraft fuel tanks were calculated to be 209 ft^3, as seen in Table 15.

Table 15. Fuel Tank Specifications

Fuel Tanks	Fuel Weight (lb)	Fuel Volume at 170 F (gal)	Tank Volume (ft^3)
Left Tank	9814	1429	209
Right Tank	9814	1429	209

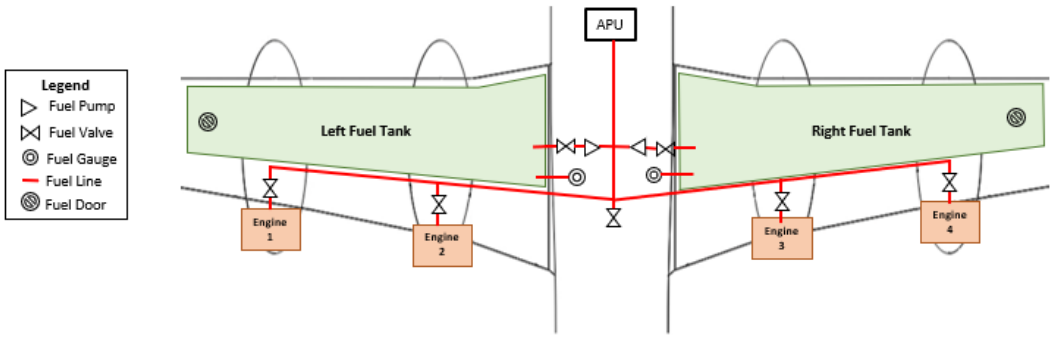

Figure 41. Fuel Systems Schematic

10.2. Hydraulic System

Hydraulics is used to actuate the control surfaces, wheel brakes, landing gear folding mechanisms, rear loading door, and fire retardant drop gate. A twin hydraulic system, shown in Figure 42 on the next page, is implemented for redundancy so that the hydraulic actuating systems can still operate in case one of the hydraulic lines fails. A cable system is also included as a backup for the hydraulic system in case of total system failure. This system will primarily be operated using the engines' hydraulic pumps although the auxiliary power unit can be used to power the backup hydraulic pump in case of failure.

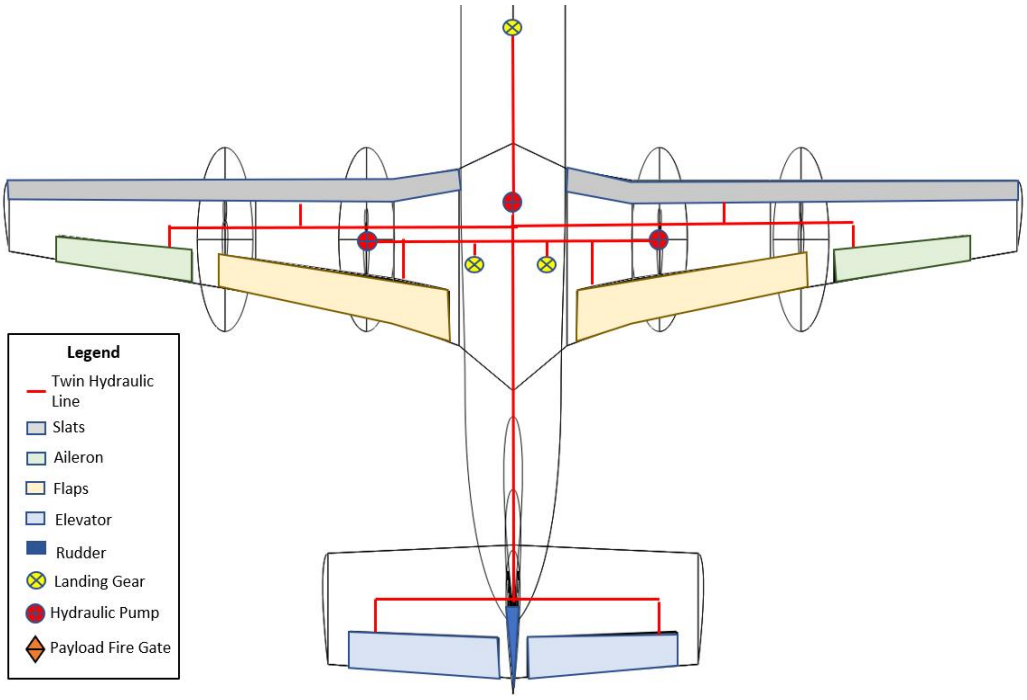

Figure 42. Hydraulic Systems Schematic

10.4. Retardant Storage/Drop System

10.4.1. Initial Design

The initial design for the payload centered around meeting the RFP requirements of an 8,000 gallon retardant capacity and multiple drops of at least 2,000 gallons. With these goals in

mind, the first iteration of the payload design featured four separate 2,000 gallon pressurized tanks situated towards the aft of the fuselage as shown in Figure 43. Each of these tanks were cylindrical in shape with a radius of 2.6 ft and a length of 13 ft. Complications with using a pressurized system, poor volume usage due to a packing factor, C.G. shifting after drops, and appropriate drop systems led to a different design choice.

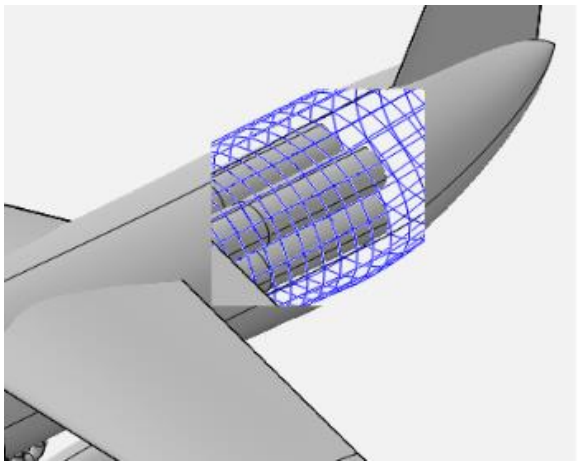

Figure 43. Original Storage Design

10.4.2 Final Tank Design

After careful consideration, the payload design aimed to shift from multiple retardant tanks to a singular, unpressurized tank centered near the C.G. This design, shown in Figure 44 on the next page, was chosen largely to reduce the unnecessary complications/weight from multiple tanks and to reduce manufacturing costs for the aircraft.

The dimensions of the tank were chosen to fit the appropriate volume of retardant needed at the minimum weight possible while still maintaining structural integrity. The material chosen was Aluminum 2024 for its high strength to weight ratio and its resistance to corrosion. The whole apparatus is situated on removable supports that bolt into the cargo floor above the fire gate. To increase ease of access, the cargo floor has integrated rollers along the center to

allow for quicker loading and unloading of not only the retardant tanks but any other components needing to be carried by the craft.

To reach the appropriate refill rate of greater than 500 gal/min, the retardant tank features two 2 ½ inch inner diameter hoses that can be used to externally fill the tank from connections along the belly of the craft. These hoses were chosen to match the diameter of most ground-based firefighting services and the reloading bases at Peterson and McClellan Air Force Bases where the DC-10 Air Tanker and C-130 MAFFS are reloaded. Each of these hoses typically have flow rates between 250-500 gal/min in land based firefighting roles, so two should sufficiently meet the reload requirement of the RFP. The tank specifications are summarized in Table 16.

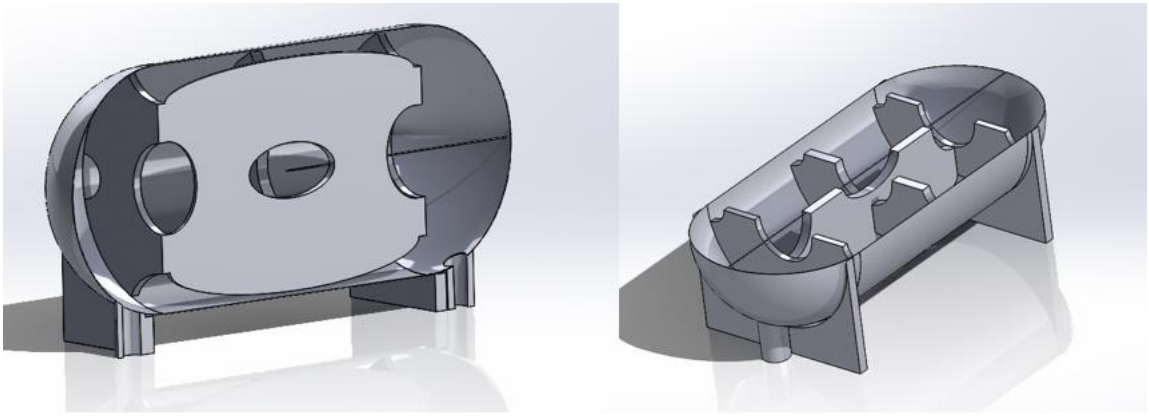

Figure 44. Section Views of Retardant Tank CAD Model

Table 16. Retardant Tank Specifications

Length (ft.)	Radius (ft.)	Wall Thickness (in.)	Volume (gal.)	Weight (lb.)	Reload Rate (gal/min)
22.74	4.14	0.19	8063	1984.16	~600

10.4.3. Baffling System

A baffling system was developed to prevent C.G. shifting during dropping maneuvers and inertial coupling during cruise. Several different designs for baffling systems were considered including traditional baffle walls, repositionable bulkheads, and baffle balls. Baffle

balls, as shown by Ahmed et al. (2022), were considered due to their low-weight and superior mitigation of inertia. However, concerns about long term resiliency of these balls and the design of a grated fire gate drop system led to the decision to continue with traditional baffle walls. Two baffle walls were positioned with a lateral orientation to prevent C.G. shifting during pitching maneuvers, and one baffle wall was placed with a longitudinal orientation to prevent weight shifting during rolling maneuvers.

10.4.4. Drop System

To simplify production costs, the GEN II Fire Retardant Dispersal System by Trotter Controls was chosen to operate the aircraft's fire gates. The FRDS GEN II is capable of modifying how the gallons dropped by partial opening and closing of the fire-gates within milliseconds to ensure appropriate drop volumes. This system was originally designed for the AT-802F, another single tank firefighting aircraft. With this in mind, the fire gates will sit along the 14.5 foot cylindrical mid-portion of the retardant tank. By choosing to use existing electronic and hydraulic systems, design costs and production costs can be reduced and reliability can be maintained without the potential failures of an in-house solution.

Figure 45. Fire Retardant Control System Gen II

10.4.5. Retardant Selection

While comparing the various retardants that could be dropped by our aircraft, we ultimately decided that Phos-Chek LC95 would be the optimal choice. There are concerns about Phos-Chek LC95 potentially being harmful to wildlife in the environment such as local fish and amphibians, but for cost concerns and firefighting efficacy it is unmatched. Hopefully in the future more biodegradable and environmentally friendly retardants could be considered as alternatives, but in the best interest of operator costs it was determined that the widely used and reliable LC95 should be chosen.

The fire retardants have large concentrations of ammonia and phosphate with moderate amounts of salt (Scauzillo, 2016). The fire retardants have been shown to be not harmful to humans and other mammals. It does cause skin and eye irritation / drying when in contact and people must wash their skin and eyes thoroughly to avoid further hindrance. The ammonia and phosphate do have detrimental effects on aquatic life. The chemicals are toxic, killing fish and other life. It also catalyzes algae blooms which can further hurt the aquatic ecosystem, drowning aquatic organisms from oxygen. It is recommended that Phos-Chek LC95 is not released 300 ft from bodies of water. The salt content in fire retardants can dry out and burn vegetation in forests if left. It is also suggested that water is dropped on the fire-extinguished sites where fire retardant was initially dropped to dilute the salt, ammonia, and phosphate amounts in both the local ecosystem and community.

10.5. Electrical System

The aircraft is equipped with four separate starter-generator units, one on the accessory drive of each engine. For auxiliary power and as an emergency system for engine failure, an auxiliary power unit, APU, is fitted behind the cockpit. The generated electrical power is utilized

to power key electrical functions of the aircraft such as actuating systems, de-icing systems, and other high-power electronics. A transformer is featured to down step the high power to a lower level to provide electricity to flight instruments and displays in the cockpit, low power electronics, and other electrical instruments. The aircraft also features redundancy of electrical safety critical systems (SCSs) and electrical wiring for added safety. If the primary electrical lines fail, the secondary electrical lines will still allow the aircraft electronics to operate. The SCSs that require constant power also have a backup battery in case of complete power failure.

The APU that the aircraft will be equipped with is the Honeywell GTCP331-200. This APU has the highest power-to-weight ratio in its class and is fitted for other aircraft of similar size and weight. This APU will be a secondary power source and will be more than enough to sustain the aircraft's energy requirements in the case of an engine failure.

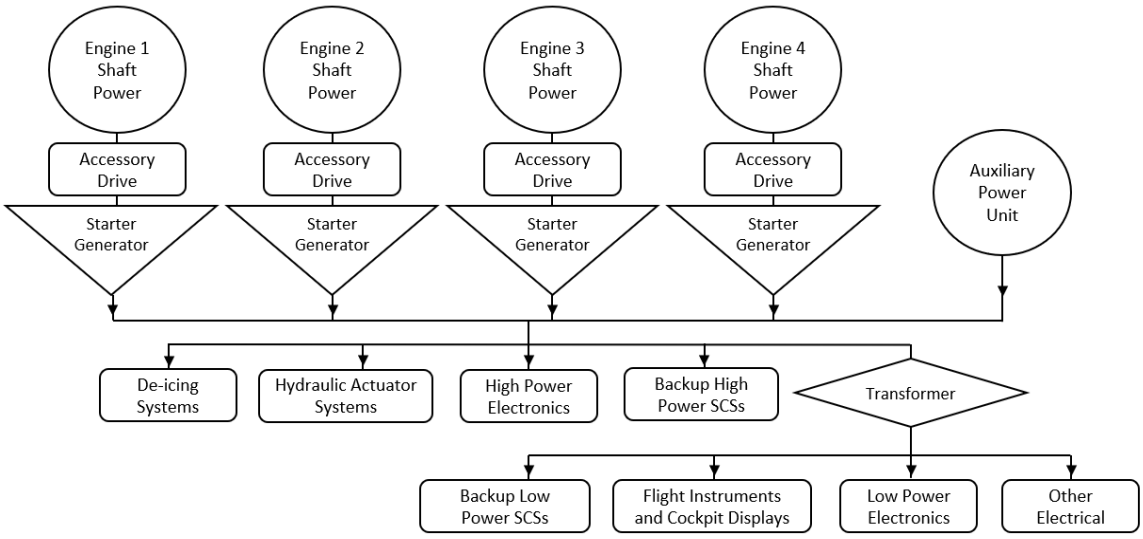

Figure 46. Electrical Systems Flow Diagram

10.6. Deicing System

The aircraft features an electro-thermal de-icing system on the leading edge of the wing and empennage. A pneumatic de-icing system was not selected due to the added weight of

integrating high pressure, bleed air lines and pumps into the airframe. The electro-thermal system offers a lower volume and lower weight solution with no significant loss in performance. Engine and propeller blade de-icing systems were not considered a genuine concern. A layer of hydrophobic paint coat will be applied to the leading-edge surfaces to reduce ice formation probability.

Low volume heating panels are embedded on the length of the leading edges which are connected to the central electrical system and cockpit controls. A microwave resonator sensor is integrated in the de-icing system to detect ice buildup on the leading edges in real time and to automatically enable and disable the heating mechanism in an energy-efficient manner. The use of carbon nano tube (CNT) films or graphene heating elements for de-icing are also considered.

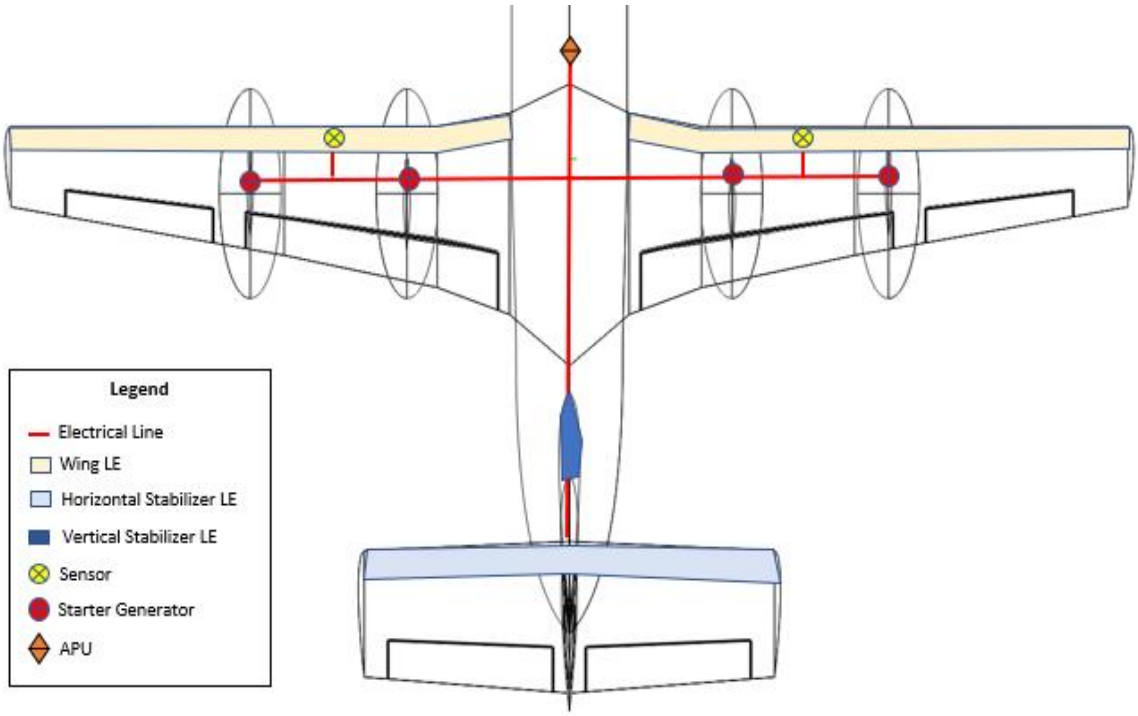

Figure 47. De-icing System Schematic

10.7. Avionics and Sensors

Under FAA § 91.205 Powered civil aircraft with standard category U.S. airworthiness certificates: Instrument and equipment requirements:

VFR flight during the day, the instruments and equipment required are: an airspeed indicator, an altimeter, a magnetic direction indicator, a tachometer for each engine, an oil pressure gauge for each engine using pressure system, a temperature gauge for each liquid-cooled engine, an oil temperature gauge for each air-cooled engine, a manifold pressure gauge for each altitude engine, a fuel gauge indicating the quantity of fuel in each tank, a landing gear position indicator if the aircraft has retractable landing gear, approved flotation gear for each occupant, and an approved safety belt with an approved metal-to-metal latching device or other restraint system for each occupant 2 years of age or older (Federal Aviation Administration, 2017).

For VFR flight at night, the instruments and equipment required are: the instruments and equipment for VFR flight during the day, approved position lights, an approved aviation red or aviation white anti-collision light system, one electric landing light if the aircraft is operated for hire, an adequate source of electrical energy for all installed electrical and radio equipment, and one spare set of fuses, or three spare fuses of each kind required, that are accessible to the pilot in flight. For IFR flight, the instruments and equipment required are: the instruments for VFR flight during the day and at night, two-way radio communication and navigation equipment suitable for the route to be flown, gyroscopic rate-of-turn indicator, slip-skid indicator, sensitive altimeter adjustable for barometric pressure, a clock displaying hours, minutes, and seconds with a sweep-second pointer or digital presentation, generator or alternator of adequate capacity, gyroscopic pitch and bank indicator, and gyroscopic direction indicator. The aircraft will be installed with the FAA required instruments and equipment (Federal Aviation Administration, 2017).

The aircraft will be able to detect forest fires using live video detection. This will be done through the use of existing methods of detecting forest fires using algorithms. The process for one method of detection of a forest fire starts off with image acquisition which can come in the form of individual images or a series of video frames. From here, the images are extracted for color components in the form of red, green, and blue. Then the values for the color components are normalized to achieve better robustness against different lighting conditions. These normalized values can then be calculated into indices to detect fires or forest fires in the form of FDI (Fire Detection Index) and FFDI (Forest Fire Detection Index) respectively. FDI is an index used to determine whether a fire is present in the image by finding traces of orange and red in the image and differentiating it from the environment. FFDI is an index used to determine whether a forest fire is present in the image by finding traces of gray and green and differentiating between smoke and green tones of the background. These indices are then binarized to separate the important parts of the image from the background. This is done by giving the areas with indices greater than the Forest Fire Detection Threshold (FFDT), which is a value that was calculated to determine whether a fire or smoke is present, a value of 1 and the areas with indices less than the FFDT a value of 0. A value of 1 is a white color and a value of black is 0. This should result in a black and white image that showcases the smoke and fire in the image. After this, the image is then segmented and labeled, indicating where the smoke is and where the fire is in the image. All of these steps can be seen in Figure 48 below. The final image is segmented and provides the necessary information of the position of this forest fire in the image.

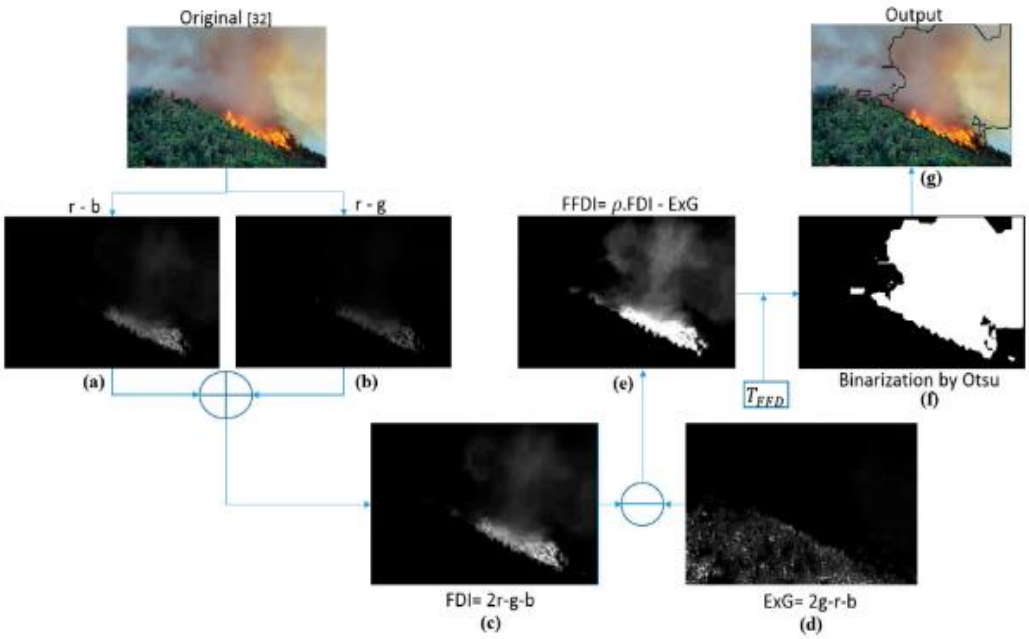

Figure 48. Diagram showing the process in which an image is analyzed for the detection of fire and smoke.

The method explained above achieved an overall detection rate of 96.84% on 1920x1080 resolution and a maximum frame rate of 54 frames per second. This method has also been proven to be effective in both distant and close views. We decided that this would be the best option for the aircraft because it is a modern solution that is better than the alternatives. An alternative is video surveillance for forest fire detection which has drawbacks that will impede the efficiency and effectiveness of the airplane. Video surveillance for forest fire detection was one of the first methods for detecting forest fires so it would present limitations in detection due to confusions in classification. This method was also designed for fixed environments which is not what this aircraft needs (Cruz et al, 2016).

The aircraft will also be fitted with Forward Looking InfraRed, FLIR, cameras so fires and smoke can still be detected in low visibility. The use of infrared cameras has benefits during the day and at night. During the day, fires typically are most abundant and intense in the early to

late afternoon and provide a very strong heat signal. While smoke is also more abundant during the day, smoke is basically undetectable at the infrared wavelengths. During the night, the contrast of flame to the background is increased due to the lack of solar heated objects which leads to a decrease in false positives. The use of a FLIR camera offers the pilot the ability to still navigate and map the terrain even when human sight visibility is poor (Allison et al, 2016).

10.8. Environmental Control Systems

This aircraft's environmental control systems, ECS, will ensure that the crew inside the aircraft will have a pressurized and thermal controlled environment. When it comes to the pressurization of the aircraft, the aircraft will be equipped with the TronAir 15_7603-1000 cabin pressure test unit which will allow the crew to monitor and control the pressurization within the cabin using pressure valves within the cabin. In the case of an emergency, oxygen masks will be equipped into the aircraft as well. When it comes to the air conditioning within the aircraft, the aircraft will be equipped with the TronAir 17-7503B7000 conditioner, which will allow the crew to monitor and control the air conditioning.

11. Aircraft Weight Breakdown

The weight for all major components of the aircraft were estimated from FLOPS based on aircraft geometric parameters and mission requirements. The weights and center of gravity values for each of the components were used to conduct a balance analysis to determine the center of gravity for the whole aircraft. The weight component breakdown is shown in Table 17 below.

Table 17. Operating Empty Weight Breakdown

Component	Weight (lb)
Wing	25040
Horizontal Tail	5367
Vertical Tail	3510
Fuselage	21806
Landing Gear	10727
Propulsion Systems	24448
Control Surfaces	2223
Avionics	1149
Furnishings	2365
Hydraulics & Electricals	5223
Anti-Icing	319
Crew	915
Cargo Containers	13300
Weight Margin	10000
Total OEW	126392

The total operating empty weight (OEW) of 126,000 lb does not include mission fuel and payload. Adding on the mission fuel and payload weights, 72,000 lb and 18,000 lb respectively, results in the maximum takeoff weight of 216,000 lb. The center of gravity of the aircraft was calculated based on each weight component and their respective C.G. locations. The C.G. was determined with respect to the nose of the aircraft, and it was found to be located at 49.14 ft.

12. C.G. Travel

Given the weight breakdown performed above, associated center of gravity (C.G.) calculations, and aircraft dimensions, it is possible to approximate aircraft C.G. travel under different loading conditions. To represent the full range of potential C.G. in the course of a flight, four configurations were assessed:

1. Maximum Takeoff Weight
2. Operating Empty Weight
3. Maximum fuel, no payload weight
4. Payload, no fuel weight

The first two configurations represent the 'default' configurations, and give takeoff and near-empty, e.g. end-of-mission, balance. The second two configurations represent the logical extremes possible during flight, of near-full fuel with completely depleted or empty retardant, and near-empty fuel with completely full retardant load.

Table 18. Center of Gravity Location According to Configuration

Configuration	C.G. (ft)
Full	49.14
Fuel only	47.72
Payload only	48.90
Empty	47.39

The results reflect fairly minimal changes in C.G., but rely on approximations for the locations of fuel tanks, retardant tanks, and general aircraft systems for C.G. estimation, as might be expected for a conceptual design. The approximate placements of these components were chosen to minimize C.G. shift as much as possible.

13. Mission Analysis

The mission profile for which the aircraft was simulated in the Flight Optimization System (FLOPS) software. FLOPS is a self-described “multidisciplinary system of computer programs for conceptual and preliminary design and evaluation of advanced aircraft concepts” published by NASA. In this program, an aircraft with defined geometry and configuration parameters can be sized for a prescribed design mission subject to customizable performance constraints.

In order to define the aircraft and its parameters, information was aggregated from various external sources. The overall dimensions, wing area, etc. were acquired from designs generated in VSPAERO, and the engine performance, rendered into engine input ‘decks’, was developed using GasTurb. The mission profile was prescribed based on conventional operations of a large transport aircraft along with the mission requirements extracted from the RFP, and can be seen visually represented in Figures 1 and 2 in section 3.

Each datum from these sources was input into the requisite position in FLOPS or the accompanying engine deck, developing a model of the standard and ferry mission profiles from which to determine sizing. A rerun mission was used to confirm the sized aircraft could achieve the ferry mission.

Table 19. FLOPS Sizing and Performance Results

Configuration	Weight (lb)/Output
Operating Weight Empty	126391.7
Payload	72000
Maximum Fuel	17963.2
Gross Weight	216354.8
Reference Wing Area	2525.00 (sq. ft.)
Wing Loading	85.69 (sq. ft.)
Thrust Per Engine	25000
Engine Scale Factor	1
Thrust-Weight Ratio	0.4622

```
START
CLIMB    1
CRUISE   1          230.
CRUISE 0 3          005.
RELE       18000.0
CRUISE 0 2          020.
CRUISE 0 3          005.
RELE       18000.0
CRUISE 0 2          020.
CRUISE 0 3          005.
RELE       18000.0
CRUISE 0 2          020.
CRUISE 0 3          005.
RELE       18000.0
CRUISE 0 1          230.
DESCENT
END

&RERUN
paylod=0,
/

&MISSIN
/
START
CLIMB    1
CRUISE   1          2000.
DESCENT
END
```

Figure 49. FLOPS Mission Definition Input Code

This work formed the ‘input’ file which was fed into FLOPS to derive the ‘output’ file and its attendant estimated weights and performance parameters. Table 19 was created from data supplied through said FLOPS output file, which uses the simulated mission and aircraft to estimate required parameters to meet the mission profile. In this particular instance the payload, thrust, and wing area were set to constant values based on mission and design constraints, with the fuel, weight, and thrust-to-weight changing in iterative FLOPS cycles until reaching the final values depicted here.

14. Manufacture

The aircraft will be manufactured with outsourcing and in-house manufacturing. Aircraft components such as the fuselage, empennage, wings, and control surfaces will be manufactured in house. Specialty parts such as avionic instruments, computer systems, and fire retardant dispersal systems will be acquired from outsourced suppliers. Since the aircraft has low production volume, high complexity components, utilizing additive manufacturing techniques will greatly expedite production and reduce the fly-buy ratio. Additive manufacturing will also be utilized to manufacture low production volume, non-critical components within the airframe. Additively manufactured components will be acquired by subcontracting with additive manufacturing suppliers. The use of readily available, shelf components and standardizing the sizing of shelf parts will improve ease of manufacturability and maintenance. The aircraft will be manufactured using an assembly line method to ensure that customers will continue to get their products in a timely and organized manner. A production chain, shown in figure 49 below, is followed by fabricating parts from raw materials, assembling in-house and outsourced parts into sub-systems such as wing and fuselage, and assembling and integrating the subsystems into a final product.

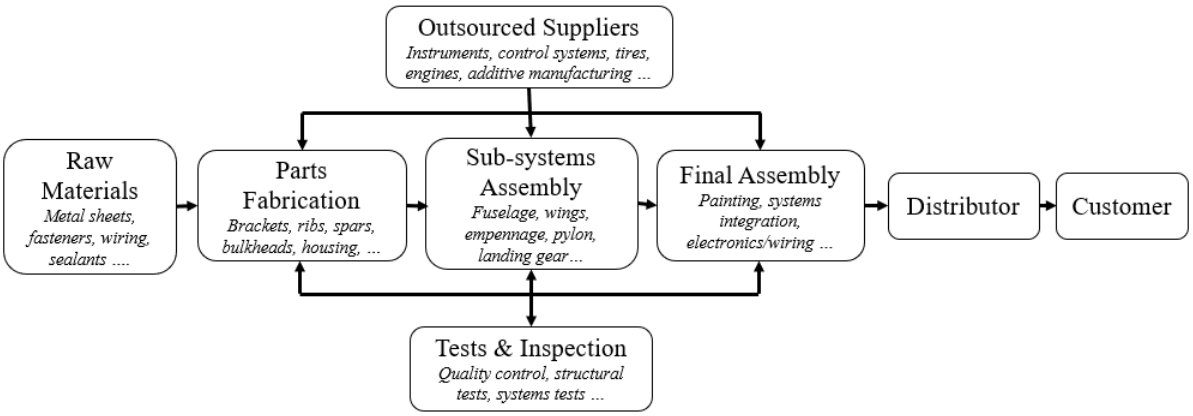

Figure 50. Manufacturing Chain

15. Maintenance

The aircraft will be maintained by certified Maintenance, Repair, and Overhaul (MRO) technicians under FAA Title 14 of the Code of Federal Regulations (14 CFR) Part 14 with a robust program of regularly scheduled, preventive inspections, servicing, testing, repair, and overhaul. This maintenance schedule will ensure airworthiness and safety for the aircraft by international standards. The aircraft will undergo routine inspections, repairs, and services to airframe components, engine components, retardant tank, instruments, hydraulic systems, fuel systems, and other components in the aircraft. The aircraft will feature access panels along the skin of both the fuselage, wing, empennage, and engine nacelle/pylon to allow technicians to easily access and inspect internal components.

The use of additive manufacturing to manufacture aircraft components will offer quick turnaround times to component replacement and repair. Direct Energy Deposition (DED) techniques may be utilized for onsite repair of broken parts. With the rapid development of Internet of Things (IoT) such as artificial intelligence and augmented reality, the implementation of wearable technology, robotic systems, and augmented reality systems will help maintenance operations and reduce any potential delays (Vazirani, n.d.).

The aircraft will typically operate in an harsh environment with low altitude flights in forest terrains, airborne debris from fire residue and forest vegetation, and strong updrafts and crosswinds. Considering these conditions and the increased cyclical loading from the mission profile, the firefighting aircraft experiences higher stresses than a typical commercial aircraft. The primary maintenance focuses for the airframe are fatigue, particulate matter build up, debris impact, and corrosion. The skin of the airframe must be regularly inspected for dents, tears, or

rips from debris impact. Since the aircraft is routinely dropping fire retardant, the fire gate door and the surrounding area must be checked on a regular basis for corrosion.

As with the rest of the fuselage, a basic step in the maintenance of the propulsion system is wiping off any particulate in the environment, particularly smoke and soot, which might rest on the surface of the propeller blades and impact their performance. Particulate matter must also be cleaned off at the air intake in order to maintain an unobstructed flow throughout the engine. Another consideration is the thermal strength of the propellers, as when flying low for the drop portion of the mission it is possible that the blades are exposed to extreme temperatures. Thus, it is important that the thermal stress the blades are able to withstand is understood, especially with respect to the long-term lifespan of the propeller.

As mentioned in section 6, the TP400 D-6 is a modular system, meaning that the components are separable, allowing for greater ease of maintenance. Moreover, if any component becomes outdated or is upgraded by the manufacturer, refitting the engine with these new parts will be a much more straightforward process. In addition, because of the international cooperation which enabled this engine design, as well as the current popularity of the engine, the availability of replacement parts should not be a limiting factor.

For the retardant system, the modularity of the unit was prioritized with maintenance in mind. The whole unit can be removed by unbolting the tank from its structural supports above the firegate and can be removed for inspection or repairing purposes. This also allows the retardant tank to be swapped with a spare during operations to continue missions. Additionally, the tank is sized in such a way that an inspector can walk around the unit between missions to inspect for damage along the external hull and to perform spot repairs should a minor crack appear.

16. Costs

16.1. Total Lifecycle Cost

A total life cycle cost analysis was performed to help understand the projected development, production, and ownership costs for the manufacturers and operators of the SB-22. To estimate the total ownership cost, the entire lifecycle of the aircraft is divided into three primary sections: R.D.T.E., Acquisition, and Operating. Each of these stages are analyzed separately with different assumptions made to reflect the market in 2030. While there are several different ways to estimate these values, the majority of the estimates used for our design come from the analytical findings of Roskam (2002) and the corresponding calculations from AAA, Advanced Aircraft Analysis.

16.2. R.D.T.E.

R.D.T.E. is the research, development, testing, and evaluation period of the aircraft. This stage deals with the creation of new technologies to be implemented in the design of the aircraft. Since this design falls within the specifications of a military class aircraft in regards to its certification and production schedule, it was modeled as such using AAA. Listed below are the assumptions made during this phase and their implications (Roskam):

- A singular flight capable test aircraft was developed as a proof of concept.
- This aircraft would be assembled over a time period of 6 months after individual components were sourced or completed.
- The materials used in the production of this test aircraft reflect standard industry material practices.
- All test avionics were representative of near-future or current technologies.
- A 15% profit margin was maintained during this stage.

Using these assumptions during this phase, a total cost of 1.522 billion dollars was estimated throughout the entire process. Additionally, the first test platform was estimated to have a cost of 572.3 million dollars. Displayed in Figure 51 is a breakdown of these costs.

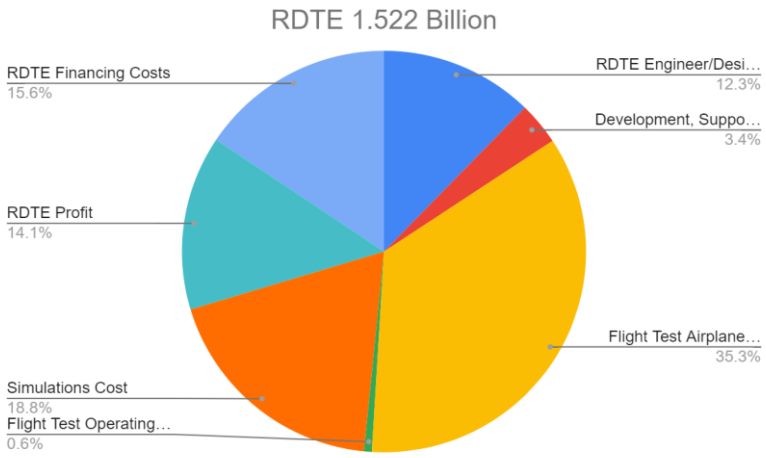

Figure 51. Breakdown of RDTE Costs

16.3. Acquisition

Acquisition costs are informed by the manufacturing and distribution phases of the aircraft and are affected by a large number of variables. Most of the aforementioned variables of the RDTE phase carry over into these phases as well as additional factors relating to the market demand for the aircraft. To determine the relative market size for this phase an analysis of comparable payload sized aircraft was conducted. From this research it was determined that approximately ten production level aircraft would be necessary. (CAL Fire) Beyond just production scale, the tooling costs, engineering costs, manufacturing labor, quality control costs, material estimates, equipment costs, and engine costs are all factored into this section. All of these factors are multiplied by their appropriate manhours estimated for the full production line life to give total costs for each position. Finally, all of these factors are scaled appropriately based on inflation rate estimates throughout this phase.

From these factors, a production model cost of $314.7 million per aircraft was estimated, with a total acquisition cost of $1.624 billion. An estimated fly-away cost can be found by looking exclusively at the manufacturing cost per aircraft and excluding all development and research costs. The flyaway costs for a production line of only ten aircraft is approximately 101.5 million. However, when this production line is increased to 100 the flyaway cost is reduced to only 37.91 should the buyer wish to pursue a larger contract. Further cost breakdown can be seen in Figure 52 below.

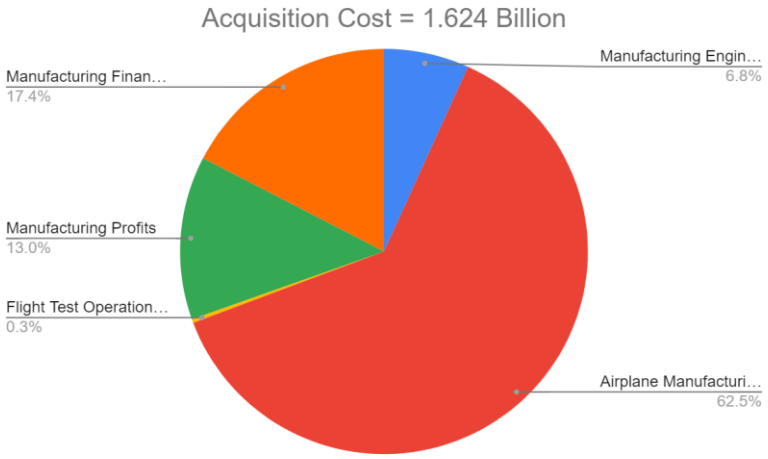

Figure 52. Breakdown of Acquisition Cost

16.4. Operation

The operation costs section deals with the actual performance of the aircraft over its intended lifespan. Major contributing factors in this section include the number of operating hours annually, the cost of fuel, costs of oil, and pilot salaries. From the RFP an estimate of 1200 annual flight hours was assumed, a cost of $4.9 per gallon of jet fuel was used based on an inflated version of current costs – a lifespan of at least 15 years was also assumed. From the current job market an average salary of $59,235 was used for each pilot and assumed crew of two was used (CAL Fire). Additionally, maintenance and ground crew costs were factored in

according to the military rates associated with AAA. A final cost of $1.217 billion for the entire operating cost of the aircraft was calculated, and an operating cost of $8.193.80 an hour was determined. This places our proposed aircraft well below the current $12,750 of a DC-10 Air Tanker. A further breakdown of costs is shown in Figure 53.

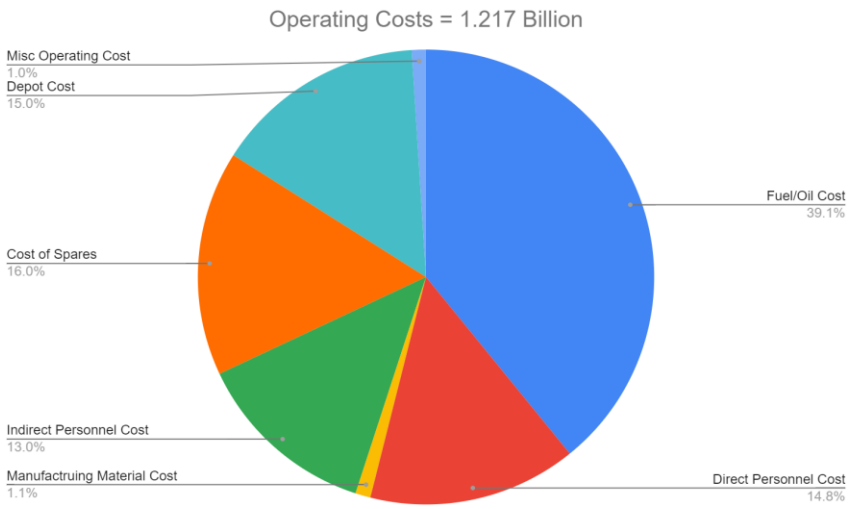

Figure 53. Operating Costs Breakdown

16.5. Disposal

Disposal of the aircraft must become a priority once the aircraft reaches the end of its life cycle either due to increased costs of operation/maintenance, legislation changes, or replacement due to obsoletion by replacement aircraft. The disposal costs of an aircraft is largely determined by the materials used in the construction of the aircraft. Certain components such as engine parts can be disassembled and reused in an engine repair network to offset the costs. Additionally, composite recycling processes can help to offset the cost of retiring the aircraft. Factoring in all these factors, an estimated disposal cost of $41.512 million for the entire fleet at the end of their life was determined.

17. Conclusion

The goal of this report was to present the steps necessary to design a very large air tanker suited for aerial firefighting that fits the requirements outlined in the Request for Proposal from the American Institute of Aeronautics and Astronautics. The number of wildfires has escalated considerably in the past decade, and the only firefighting aircraft used are still retrofitted commercial and military aircrafts. This leads to inefficiencies due to the fact that aerial firefighting missions differ starkly from commercial or military operations, and serious safety concerns due to the regular off-design, in-flight loadings experienced by modern firefighting aircraft. The SB-22 “Woodzy Owl” has been specifically designed to handle these conditions and aptly accomplishes ‘low and slow’ payload drops while maintaining maneuverability for quick dash following the release of fire retardant with the capability to loiter and prepare for multiple more payload releases.

This paper considered all of the design features and systems deemed critical to realizing the opportunity SB-22 “Woodzy Owl” concept, concluding that the aircraft is indeed flight-worthy and a compelling new product to support growing aerial firefighting fleets. Sizing analysis concluded that the aircraft can sustain the 8,000 gallon fire retardant payload capacity, while the stability and control analysis concluded that even with this payload the aircraft is still able to maneuver to complete the mission design. The propulsion analysis concluded that the four TP-400 turboprop engines provide significant thrust to keep the aircraft in the sky and allows for the necessary quick dashes prior to payload drop. The aerodynamic analysis concluded that the aircraft is capable of the necessary lift even at the low drop speeds and altitudes especially with the aid of the control surfaces on the wings and empennage. Similarly, the structures analysis then concluded that the fuselage, wing, empennage, and landing gear, are

capable of handling the associated stresses that will arise in the firefighting mission. Subsystems analysis helped to close remaining operability, certifiability, manufacturability, and maintainability gaps in the design. Finally, a thorough cost analysis showed that the SB-22 could be developed, produced, and marketed competitively relative to modern comparator aircraft. In sum, the SB-22 “Woodzy Owl” aerial firefighting airtanker is a compelling new solution designed to meet all the requirements set forth in the AIAA RFP and provide a highly-capable and affordable firefighting aircraft to bolster the aging fleets in use today.

18. References

Ahmed, S., Xin, H., Faheem, M., & Qui, B. (2022). Stability analysis of a sprayer UAV with a liquid tank with different outer shapes and inner structures. *Agriculture 2022, 12, 379.* https://doi.org/10.3390/agriculture12030379

AIAA. (2021). *Request for Proposal Responsive Aerial Fire Fighting Aircraft*.

Allison, R., Johnston, J., Craig, G., & Jennings, S. (2016). Airborne optical and thermal remote sensing for wildfire detection and monitoring. *Sensors, 16*(8), 1310. https://doi.org/10.3390/s16081310

Blaesser, N. J. (2019). *Interference drag due to engine nacelle location for a single-aisle, transonic aircraft* [Doctoral dissertation, Virginia Polytechnic Institute and State University]. VTechWorks.

California Department of Forestry and Fire Protection (CAL FIRE). (2022). *Aviation program*. Cal Fire Department of Forestry and Fire Protection. Retrieved from https://www.fire.ca.gov/programs/fire-protection/aviation-program

California Department of Parks and Recreation. (2022). *How big are big trees?*. Retrieved from https://www.parks.ca.gov/?page_id=1146#:~:text=Sierra%20redwood%20trees%20are%20the,redwood%20lies%20in%20its%20bulk

CFI Notebook. (2022). *Aircraft landing gear*. https://www.cfinotebook.net/notebook/operati on-of-aircraft-systems/aircraft-landing-gear

Cruz, H., Eckert, M., Meneses, J., & Martínez, J.-F. (2016). Efficient Forest Fire Detection index for application in Unmanned Aerial Systems (uass). *Sensors, 16*(6), 893. https://doi.org/10.3390/s16060893

Europrop International. (n.d.). *TP400-D6 engine.* http://www.europrop-int.com/the-tp400-d6/

Federal Aviation Administration. (2017). *ECFR :: 14 CFR part 91 -- General Operating and Flight Rules*. Code of Federal Regulations. Retrieved May 3, 2022, from https://www.ecfr.gov/current/title-14/chapter-I/subchapter-F/part-91?toc=1

Gabbert, B. (2014, June 29). *MD-87 air tankers recalled*. Fire Aviation. Retrieved from https://fireaviation.com /2014/06/29/md-87-air-tankers-recalled/

George, C. W. (1988). *An update on the operational retardant effectiveness (ore)program*. 114–123.

Hall, J. E., Hull, J. B., Johnson, K., McKinney Jr., E. H., & Scott, W. B. (2002). *Federal Aerial Firefighting: Assessing Safety and Effectiveness Blue Ribbon Panel Report to the Chief* (Issue December). Retrieved from https://wildfiretoday.com/documents/Blue_Ribbon_Panel_Final_12-05-2002.pdf

Langfield, M. (2021, June). *Giving old aircraft a new lease of life as aerial firefighters*. AirMed&Rescue, 117. Retrieved from https://www.airmedandrescue.com/latest/long-read/giving-old-aircraft-new-lease-life-aerial-firefighters

National Interagency Coordination Center. (2020). *Wildland Fire Summary and Statistics Annual Report*. 1–35.

Natural History Museum of Utah. *Wildfire FAQs*. Retrieved from https://nhmu.utah.edu/sites/default/files/ attachments/Wildfire%20FAQs.pdf

Nicolai, L. M., & Carichner, G. E. (2010). *Fundamentals of aircraft and airship design, volume I - aircraft Design.* American Institute of Aeronautics and Astronautics (AIAA).

OpenVSP. Parasite drag tool. (n.d.). Retrieved from http://openvsp.org/wiki/doku.php?id=parasitedrag

PilotClimb. (2021). *Balanced field length*. Retrieved from https://pilotclimb.com/balanced-field-length-balanced-v1/

Powered civil aircraft with standard category U.S. airworthiness certificates: Instrument and equipment requirements (2017).

Ratier-Figeac. (n.d.). *Propellers*. https://www.ratier-figeac.com/en/propellers

Raymer, D. P. (1992). *Aircraft design: a conceptual approach*. American Institute of Aeronautics and Astronautics (AIAA).

Roskam, J. (2002). *Airplane Design: Part Viii: Airplane cost estimation: Design, development, manufacturing and operating*. University of Kansas.

Scauzillo, S. (2016). *Is that red fire retardant dropped from planes during wildfires safe for humans and the environment?.* Retrieved from https://www.sgvtribune.com/2016/07/23/is-that-red-fire-retardant-dropped-from-planes-during-wildfires-safe-for-humans-and-the-environment/

Schaufele, R. D. (2007). *The elements of aircraft preliminary design.* Aries Publications.

U.S. Forest Service. (2020). *Aviation Annual Report 2020*. Retrieved from https://www.fs.usda.gov/

United States Department of Agriculture. (2020). *Aerial Firefighting Use and Effectiveness (AFUE) Report* (Issue March).

Vazirani, P. (n.d.). *Everything MRO: Putting Maintenance, Repair, and Overhaul on Blast.* Retrieved from https://www.chetu.com/blogs/aviation/future-of-mro-software.php